A Lagrangian analysis of a developing and non-developing disturbance observed during the PREDICT experiment

Blake Rutherford[1] **and Michael T. Montgomery**[1]

[1]Naval Postgraduate School, Monterey, CA, USA

Abstract. The problem of tropical cyclone formation requires among other things an improved understanding of recirculating flow regions on sub-synoptic scales in a time evolving flow with typically sparse real-time data. This recirculation problem has previously been approached assuming as a first approximation both a layer-wise two-dimensional and nearly steady flow in a co-moving frame with the parent tropical wave or disturbance. This paper provides an introduction of new Lagrangian techniques for locating flow boundaries that encompass regions of recirculation in time-dependent flows that relax the steady flow approximation.

Lagrangian methods detect recirculating regions from time-dependent data and offer a more complete methodology than the approximate steady framework. The Lagrangian reference frame follows particle trajectories so that flow boundaries which constrain particle transport can be viewed objectively. Finite-time Lagrangian scalar field methods from dynamical systems theory offer a way to compute boundaries from grids of particles seeded in and near a disturbance.

The methods are applied to both a developing and non-developing disturbance observed during the recent pre-depression investigation of cloud systems in the tropics (PREDICT) experiment. The data for this analysis is derived from global forecast model output that assimilated the dropsonde observations as they were being collected by research aircraft. Since Lagrangian methods require trajectory integrations, we address some practical issues of using Lagrangian methods in the tropical cyclogenesis problem. Lagrangian diagnostics developed here are used to evaluate the previously hypothesized import of dry air into ex-Gaston, which did not re-develop into a tropical cyclone, and the exclusion of dry air from pre-Karl, which did become a tropical cyclone and later a major hurricane.

Correspondence to: Blake Rutherford
(bdruther@nps.edu)

1 Introduction

1.1 The genesis problem and pouch hypothesis

The prediction of tropical cyclogenesis[1] is an important problem in tropical meteorology and geophysical fluid dynamics. While much effort has been devoted to the study of mature tropical cyclones, and their track and intensity estimates, only recently has a significant research effort been dedicated to the problem of the transformation of a tropical disturbance into a tropical depression.

A new paradigm for tropical cyclogenesis, dubbed the "marsupial paradigm", was recently developed by Dunkerton, Montgomery, and Wang (Dunkerton et al. , 2009) (hereafter DMW09). This work showed that a region of recirculation along a propagating Easterly wave occurred in all pre-genesis cases analyzed therein. The center of the sub-synoptic scale circulation, defined as the intersection of the parent wave's trough axis and the wave's critical latitude in the lower troposphere, was demonstrated to be the preferred location of cyclogenesis. The region of recirculation, coined the "pouch", protects the low- to mid-level embryonic vortex from adverse conditions, while the proto vortex within is nurtured and amplified by convection within the pouch.

---

[1]The glossary on NOAAs Hurricane Research Divisions website uses tropical cyclone as the generic term for a nonfrontal synoptic-scale low-pressure system over tropical or sub-tropical waters with organized convection (i.e. thunderstorm activity) and a definite cyclonic surface wind circulation. Notably, this definition does not invoke any wind threshold. The same glossary defines a tropical depression as a tropical cyclone with maximum sustained surface winds of less than 17 (34 kt, 39 mph) and, in the Atlantic and Eastern Pacific Basins, a tropical storm as a tropical cyclone with surface winds between $17\ ms^{-1}$ and $33\ ms^{-1}$. In this study we will define genesis as the formation of a tropical depression and we impose no formal threshold on wind speed.

		Form Approved
Report Documentation Page		*Form Approved OMB No. 0704-0188*

Public reporting burden for the collection of information is estimated to average 1 hour per response, including the time for reviewing instructions, searching existing data sources, gathering and maintaining the data needed, and completing and reviewing the collection of information. Send comments regarding this burden estimate or any other aspect of this collection of information, including suggestions for reducing this burden, to Washington Headquarters Services, Directorate for Information Operations and Reports, 1215 Jefferson Davis Highway, Suite 1204, Arlington VA 22202-4302. Respondents should be aware that notwithstanding any other provision of law, no person shall be subject to a penalty for failing to comply with a collection of information if it does not display a currently valid OMB control number.

1. REPORT DATE **SEP 2011**	2. REPORT TYPE	3. DATES COVERED **00-00-2011 to 00-00-2011**
4. TITLE AND SUBTITLE **A Lagrangian analysis of a developing and non-developing disturbance observed during the PREDICT experiment**		5a. CONTRACT NUMBER
		5b. GRANT NUMBER
		5c. PROGRAM ELEMENT NUMBER
6. AUTHOR(S)		5d. PROJECT NUMBER
		5e. TASK NUMBER
		5f. WORK UNIT NUMBER
7. PERFORMING ORGANIZATION NAME(S) AND ADDRESS(ES) **Naval Postgraduate School,Department of Meteorology,Monterey,CA,93943**		8. PERFORMING ORGANIZATION REPORT NUMBER
9. SPONSORING/MONITORING AGENCY NAME(S) AND ADDRESS(ES)		10. SPONSOR/MONITOR'S ACRONYM(S)
		11. SPONSOR/MONITOR'S REPORT NUMBER(S)

12. DISTRIBUTION/AVAILABILITY STATEMENT
Approved for public release; distribution unlimited

13. SUPPLEMENTARY NOTES

14. ABSTRACT
The problem of tropical cyclone formation requires among other things an improved understanding of recirculating flow regions on sub-synoptic scales in a time evolving flow with typically sparse real-time data. This recirculation problem has previously been approached assuming as a first approximation both a layer-wise two-dimensional and nearly steady flow in a co-moving frame with the parent tropical wave or disturbance. This paper provides an introduction of new Lagrangian techniques for locating flow boundaries that encompass regions of recirculation in timedependent flows that relax the steady flow approximation. Lagrangian methods detect recirculating regions from time-dependent data and offer a more complete methodology than the approximate steady framework. The Lagrangian reference frame follows particle trajectories so that flow boundaries which constrain particle transport can be viewed objectively. Finite-time Lagrangian scalar field methods from dynamical systems theory offer a way to compute boundaries from grids of particles seeded in and near a disturbance. The methods are applied to both a developing and nondeveloping disturbance observed during the recent predepression investigation of cloud systems in the tropics (PREDICT) experiment. The data for this analysis is derived from global forecast model output that assimilated the dropsonde observations as they were being collected by research aircraft. Since Lagrangian methods require trajectory integrations, we address some practical issues of using Lagrangian methods in the tropical cyclogenesis problem. Lagrangian diagnostics developed here are used to evaluate the previously hypothesized import of dry air into ex-Gaston which did not re-develop into a tropical cyclone, and the exclusion of dry air from pre-Karl, which did become a tropical cyclone and later a major hurricane.

15. SUBJECT TERMS

16. SECURITY CLASSIFICATION OF:			17. LIMITATION OF ABSTRACT	18. NUMBER OF PAGES	19a. NAME OF RESPONSIBLE PERSON
a. REPORT **unclassified**	b. ABSTRACT **unclassified**	c. THIS PAGE **unclassified**	**Same as Report (SAR)**	**107**	

The three main hypotheses of the marsupial paradigm can be summarized as follows:

1. The cat's eye region within the critical layer has cyclonic recirculation with little strain deformation, and its center serves as the focal point for vorticity aggregation of convectively generated vertical vorticity and their vortical remnants.

2. Air inside the cat's eye is repeatedly moistened by convection and is protected to some extent from the lateral intrusion of dry air.

3. The parent wave is maintained and possibly enhanced by convectively amplified mesoscale eddies within the wave.

1.2   The PREDICT experiment

The marsupial paradigm was tested in part during the Pre-Depression Investigation of Cloud systems in the Tropics (PREDICT) experiment. The PREDICT experiment was designed to investigate the problem of genesis during the 2010 Atlantic hurricane season through a series of flights into and data analysis of developing and non-developing tropical disturbances. Along with flight-level and dropsonde data, observational satellite data was analyzed and an ensemble of numerical weather forecast models were run each day during the experiment. A description of the overall experiment, as well as a summary of some first results, is given by Montgomery et al. (2011).

In a follow-up paper, Smith and Montgomery (2011) carried out a more in-depth analysis of the convective environment in a subset of developing and non-developing tropical disturbances during the last four week period of the experiment. In all systems, there is a tendency for the lower troposphere to moisten, but in the system that did not develop, the middle and upper troposphere became progressively drier during the five missions. The most prominent difference between the non-developing system and the two systems that developed was the much larger reduction of equivalent potential temperature between the surface and a height of 3 km, typically 25 K in the non-developing system, compared with only 17 K in the systems that developed. Conventional wisdom would suggest that, for this reason, the convective downdraughts would be stronger in the non-developing system and would thereby act to suppress the development. Smith and Montgomery (op. cit.) presented an alternative hypothesis that the drier mid-level air weakens the convective updraughts and thereby weakens the amplification of system relative vorticity necessary for development. Although detailed testing of the alternative hypothesis is forthcoming (Kilroy and Smith, personal communication), the findings of Montgomery et al. (2001) and Smith and Montgomery (2011) raise the important question of what caused the progressive drying for the non-developing disturbance and what

prevented drying in the developing disturbances? As argued in DMW09, the answer to this question requires the realization of the Lagrangian nature of the genesis problem and the importance of identifying intrinsic flow boundaries that limit/enable the transport and mixing of adiabatic invariants between the potential development region with its environment. One of the outcomes of this work will be an explanation of the drying in the non-developing disturbance and the moistening in one of the developing disturbances.

1.3   Lagrangian aspects of genesis

The Lagrangian nature of the problem is most readily exposed in the moving reference frame following the path of an Easterly wave. By subtracting the wave propagation speed, the Lagrangian reference frame provides a velocity field with cyclonic recirculation in the wave trough at sufficiently large wave amplitude.

The Lagrangian reference frame is implicitly used by observational meteorologists tracking features or storms. The Lagrangian reference frame can be used to locate persistent flow boundaries, and has become a powerful diagnostic tool in the past decade in the dynamical systems community. However, these new methods are not well known to the meteorological community. Both communities accept that Lagrangian coherent structures (LCSs) generally refer to any flow structure which is coherent through the time-varying flow in the Lagrangian reference frame. However, more precise definitions of LCSs for time-dependent flows have been provided recently by the dynamical systems community.

In this study, Lagrangian kinematic aspects of the pouch theory are explored by an analysis of trajectory motion and scalar fields derived from trajectory motion using methods from dynamical systems. The maximal ridges of scalar fields are LCSs that form finite-time boundaries and govern the mixing and transport of tracers (Shadden et al. , 2005; Haller and Yuan , 2000). The stirring, which is modulated by the LCSs, shows the pathways for the entry of air into a candidate disturbance or pre-storm.

The role of structures and boundaries is important for understanding the transport of moisture and absolute vertical vorticity, two important elements in the genesis of a tropical cyclone (DMW09). Considering this problem in time-dependent velocity fields could ultimately lead to better prediction of cyclogenesis. The use of Lagrangian methods on atmospheric data, see e.g. Huber et al. (2001); Tang et al. (2009), has so far been limited for a variety of reasons, including lack of available data and lack of collaboration.

1.4   The objective pouch identification problem

The study of kinematics of trajectory motion during genesis is important for validating both aspects of the second hypothesis of the marsupial paradigm for candidate disturbances. One the one hand, the second hypothesis requires Lagrangian

recirculation along the travelling parent wave to protect the pouch. Recirculation of fluid parcels in a time-dependent flow does not necessarily occur in regions of instantaneous positive cyclonic vorticity, but only occurs when the parcel remains entrained for a sufficiently long time. On the other hand, the second hypothesis also requires that the lateral intrusion of dry air be minimal. Both of these criteria can be verified by finding persistent boundaries at the edge of the primary circulation which allow recirculation within the vortex and limit interaction from the environment.

The OW criterion (as defined herein) and vorticity are Eulerian measures of rotation commonly used in atmospheric predictions and analysis. Vorticity is defined mathematically as the curl of the velocity field and represents twice the local rotation rate of a fluid particle. The Okubo-Weiss (OW) criterion helps characterize vortex resilience by measuring the relative role of vorticity in relation to strain and shear, and helps reveal particles that have high vorticity and low strain deformation and remain entrained in vortices.

In the cases studied during PREDICT, the time-variation of the translation speed was sometimes sufficiently large that streamlines did not exhibit consistently closed circulation under small variations in the translation speed. The Eulerian methods are sensitive not only to the time-change of translation speed but also the time-change in fluid velocities. To better understand recirculation in a moving frame of reference, we consider a wave-pouch defined objectively in a moving frame of reference along particle trajectories that is Galilean invariant (independent of translations, rotations, and time-dependence of the flow) and avoids many of the approximations employed previously in the observational and modeling studies testing the pouch theory. In addition, objective measures do not require the location of a pouch center or the computation of the pouch translation speed.

1.5 Lagrangian methods for time dependent flows

Determining objective kinematic properties has been recently the subject of some extensive work in dynamical systems research. The studies of the kinematics of trajectory motion can be classified as either exact computation of kinematic boundaries or the statistics of trajectory motion.

Kinematic boundaries

Much recent research has focused on locating persistent kinematic boundaries in time-dependent fluid flows represented as data sets. The boundaries which control tracer transport are related to the stable and unstable manifolds of a hyperbolic fixed point, or a saddle-point. If the flow is steady, the manifolds partition the flow, but are distinguished from other streamlines since they show maximal linear instability for particles located close to the manifolds. Time-dependent analogs of the saddle point and manifolds were shown by Duan and Wiggins (1996) and Ide et al. (2002) to con-

trol particle transport and persist in time-dependent flows. These finite-length manifolds are the material lines which show maximal linear stability/instability for finite times. The time-dependent saddle, which is the intersection of the stable and unstable manifolds, is called a hyperbolic trajectory and is associated with persistent though not necessarily fixed stagnation points of the steady flow. The algorithms used to locate the manifolds are sensitive to the time-dependence of the flow and the persistence of stagnation points.

Finite-time Lagrangian methods were developed by Haller and coauthors (Haller and Poje , 1997; Haller , 2001; Haller and Yuan , 2000) as an efficient way of directly locating kinematic boundaries without computing a hyperbolic trajectory. These studies showed that the most persistent boundaries were material lines which tended to have maximum times of linear instability. The specific material lines that act as the most persistent boundaries can be seen as maximal ridges in Lagrangian scalar fields, which measure finite-time separation directly from particle trajectories. LCSs are robust under time-variation of fluid velocities (Shadden , 2006), and velocity approximations (Haller , 2002), though the loss of hyperbolicity of the underlying saddle trajectory may alter the invariance of the LCS (Branicki and Wiggins , 2010). These methods have proven useful in a variety of geophysical flows, see e.g. Salman et al. (2008); Tang et al. (2009).

Kinematic boundaries near a recirculating flow region

The specific application of finite-time Lagrangian methods in this study is to understand the kinematic boundaries near a two-dimensional recirculating flow region, or wave-pouch as described above. Pertinent to this theme, the hyperbolic manifolds for a steady tropical cyclone vortex were studied by Riemer and Montgomery (2011), and were shown to influence the import of dry air to the inner-core of the vortex. Similar boundaries were found during the PREDICT experiment by Evans et al. (2011). The finite-time boundaries that we present here from the PREDICT experiment often differ from Eulerian streamlines and the manifolds found in Evans et al. (2011).

1.6 Summary

The outline of this paper is as follows. In Section 2, we provide an introduction to Lagrangian methods for time-dependent flows, and show how they can be made applicable to the flows considered during the PREDICT experiment. Section 3 provides numerical details of the Lagrangian computations as well as numerical details about the data obtained from the PREDICT experiment. Sections 4 and 5 present the primary results of this study. In Section 4, we consider the nature of time-dependence of fluid velocities during pre-genesis conditions and contrast Lagrangian boundaries to Eulerian streamlines. In Section 5, Finite-time Lagrangian methods and Lagrangian statistical methods are applied to a

developing and a non-developing disturbance. The LCSs are shown to be important for controlling the import of dry air into the core for a non-developing disturbance, and protecting the core of a developing disturbance. Conclusions and a future outlook are provided in Section 6.

2 Overview of Lagrangian methods

Lagrangian methods were developed to analyse the interaction of particles with flow boundaries, which guide their movement. The need to generalize the boundaries of a steady flow to time-dependent flows led to the development of finite-time Lagrangian methods. For vortex dominated flows, time-scale finite-time Lagrangian methods were introduced. When the boundaries are difficult to see due to turbulence, statistical measures of trajectory motion give insight into the mixing and transport processes.

Since finite-time Lagrangian methods have been developed relatively recently and have not yet appeared in the tropical meteorology literature we provide here a basic introduction on the flow geometry associated with a hyperbolic fixed point for two-dimensional steady flows, and present a basic theory of some common finite-time Lagrangian methods and statistical methods.

Hyperbolic fixed point and manifolds

Assume that a velocity field $\mathbf{u}(\mathbf{x})$, $\mathbf{x} \in \mathbb{R}^2$ is steady. A fixed point $\mathbf{x}_h$ is a point where velocities vanish, $\mathbf{u} = 0$. We are concerned only with fixed points having hyperbolic or saddle-type stability. Hyperbolicity is a property of the linearized velocity field,

$$\dot{\xi} = \partial_x(\xi), \tag{1}$$

and is defined by $\nabla_x(\mathbf{x}_h)$ having eigenvalues of opposite signs, showing a direction of expansion and contraction. The stable manifold is the solution that converges to the hyperbolic fixed point along the eigendirection of the positive eigenvalue. The unstable manifold diverges from the hyperbolic fixed point in the eigendirection of the negative eigenvalue or converges backward in time. The stable and unstable manifolds are important solutions because they form a partition of the flow, which distinguish them from generic streamlines. Particles near the stable manifold travel toward the unstable manifold near the fixed point. The stable manifold is repelling to nearby particles while the unstable manifold is attracting, (Haller and Yuan , 2000).

Time variation, hyperbolic trajectories, and lobe dynamics

Invariant manifolds may still exist in a time-dependent flow and have the same local kinematic properties as in a steady flow. The intersection of time-varying manifolds is called

a distinguished hyperbolic trajectory (DHT), which is a solution that maintains linearized hyperbolic stability, with eigenvalues of opposite signs at each time. DHTs are often marked by persistent hyperbolic stagnation points at each fixed time, and are the time dependent analog of the hyperbolic stagnation point. The stable and unstable manifolds of the DHT are the particle trajectories that converge forward/backward in time to the DHT(Ide et al. , 2002). The manifolds are distinguished for time-dependent flows in that they are not crossed by trajectories, and form flow boundaries in time-dependent flows in the same manner that velocity streamlines do for steady flows (Malhotra and Wiggins , 1999; Coulliette and Wiggins , 2000). An algorithm by Mancho et al. (2003) may find manifolds if the time-dependence of the velocity field is small, though in general, manifolds in time-dependent flows are difficult to compute.

Time-dependent flows may show much more complex geometry away from the DHT. Stable and unstable manifolds are allowed to intersect at points other than the DHT. Contained regions formed by the transverse intersections of the manifolds are called lobes. Lobe dynamics describes the transport of material contained within the lobes.

2.1 Finite-time Lagrangian methods

Computing DHTs and their manifolds is often difficult, particularly in the absence of persistent stagnation points. Finite-time Lagrangian methods avoid this difficulty by finding the manifolds directly For a time-dependent flow, consider two nearby trajectories straddling a manifold. It is expected that these trajectories experience more relative separation than generic pairs of trajectories. Finite-time Lagrangian methods measure this separation and show LCSs which correspond to manifolds as the regions of maximal separation. Though the DHT is not computed directly, it can be identified as the intersection of stable and unstable manifolds.

Lagrangian scalar fields

Finite-time Lagrangian methods compute Lagrangian scalar fields on a grid of initial conditions. Lagrangian values are assigned the the initial position $\mathbf{x}_0$. Let $\mathbf{x}_0 \mapsto \phi_{t_0}^t(\mathbf{x}_0)$ be the flow map associated with the ordinary differential equation for fluid velocities

$$\dot{\mathbf{x}} = \mathbf{u}(\mathbf{x}, t) \tag{2}$$

governing the location of particle trajectories $\mathbf{x}(\mathbf{x}_0, t_0, t)$, that is, the solution of (2) with initial condition $\mathbf{x}(t_0) = \mathbf{x}_0$. Note that for finite-times, $\delta t = t - t_0$ is the chosen integration time. Small perturbations in the initial condition, $\mathbf{y}_0 = \mathbf{x}_0 + \boldsymbol{\xi}_0$, lead to a perturbed trajectory $\mathbf{y}(t) = \mathbf{x}(t) + \boldsymbol{\xi}(t)$. For sufficiently small $|\boldsymbol{\xi}_0|$, the perturbation $\boldsymbol{\xi}(t)$ can be approximated through the Jacobian of the flow map as

$$\boldsymbol{\xi}(t) = d_{\mathbf{x}_0} \phi_{t_0}^t(\mathbf{x}_0) \boldsymbol{\xi}_0, \tag{3}$$

which satisfies the variational equation

$$\dot{\boldsymbol{\xi}} = \nabla \mathbf{u}(\mathbf{x}(t), t)\boldsymbol{\xi}. \qquad (4)$$

Finite time Lyapunov exponents

Finite time Lyapunov exponents have become a standard diagnostic for Lagrangian trajectory separation (Shadden , 2006; Haller , 2002). Consider a time range $[t_0, t_0 + \delta t]$ with fixed integration time δt. The growth of $|\boldsymbol{\xi}(t)|$ during this time range is governed by the Cauchy-Green deformation tensor,

$$\Delta(\mathbf{x}_0, t_0, t_0 + \delta t) = \left(d_{\mathbf{x}_0}\phi_{t_0}^{t_0+\delta t}(\mathbf{x}_0)\right)^* \left(d_{\mathbf{x}_0}\phi_{t_0}^{t_0+\delta t}(\mathbf{x}_0)\right),$$

and becomes maximal when $\boldsymbol{\xi}_0$ is aligned with the eigenvector corresponding to the larger eigenvalue, $\lambda_{\max}(\Delta)$, of Δ. The quantity

$$\sigma(\mathbf{x}_0, t_0, t_0 + \delta t) = \frac{1}{2|\delta t|} \ln \lambda_{\max}(\Delta(\mathbf{x}_0, t_0, t_0 + \delta t))$$

is the FTLE (considered as a function of $\mathbf{x}_0$) at the initial time t_0, and the FTLE-field evaluates the FTLE on a grid of initial conditions. Repelling and attracting LCSs are maximal ridges of the forward ($\delta t > 0$) and backward ($\delta t < 0$) FTLE-fields, which play the role of stable and unstable manifolds over the finite integration time (Haller , 2000; Shadden et al. , 2005).

Lagrangian methods for vortices

The tendency for a wave-pouch region to resist strain can be described by Lagrangian measures of vorticity. Lagrangian measures, which highlight the rotational flow component depart from Lagrangian strain metrics by viewing the total time that kinematic properties persist rather than measuring the magnitude of deformations (Haller and Yuan , 2000). These Lagrangian time-scale methods include finite-size Lyapunov exponents (FSLEs), which are derived from the time required for separation of a finite distance. Let $D > 1$ be the factor of separation of initial particles, and T_D the time required for nearby trajectories to separate by this factor. By switching the time and length scale, the FSLE is defined as

$$\lambda_S \approx \log D \frac{1}{T_D} \qquad (5)$$

FSLEs are particularly useful in oceanic and vortex flows (d'Ovidio et al. , 2004, 2009), but have the disadvantage of being parameter dependent. It should be noted that though FSLEs often show comparable LCSs as FTLEs, they are purely a diagnostic (Branicki and Wiggins , 2010).

Lagrangian vortices can be found by time-scale methods as regions where strain deformation is dominated by rotation for the longest times (Haller and Yuan , 2000; Haller , 2005), and can be considered a Lagrangian Okubo-Weiss

criterion. Haller (2005) provided an objective definition of a vortex using a Lagrangian coordinate system along particle trajectories for a three-dimensional flow, while Lapeyre et al. (1999) provided a generalized OW criterion which incorporates time-dependent terms. Comparisons of OW with FSLEs have been studied by d'Ovidio et al. (2004) for oceanic vortices. As an example of some of the new tools introduced here, we compare FSLEs and other related Lagrangian metrics to the OW criterion.

2.2 Statistical methods

Aggregate information about the Lagrangian transport can be contained in trajectory statistics if the flow is turbulent. Measures such as relative dispersion and velocity autocorrelations (Weiss and Provenzale , 2008) can be adapted to characterize the wave-pouch in a moving frame. The time evolution of statistical measures can be compared to the time evolution of quantities such as vorticity or the Okubo-Weiss parameter or vorticity. Velocity autocorrelations show the amount of time that particles maintain their velocity, and provide a measure of the time-dependence of the flow. A comparison of autocorrelations of different Lagrangian and Eulerian quantities will help discern which quantities are more useful for predicting future movement, and will demonstrate that the Lagrangian reference frame has certain advantages over the Eulerian frame.

Autocorrelation function

The time-dependence of the flow can be characterized by the autocorrelation function. The autocorrelation function of a scalar quantity for a set of trajectories determines how the trajectories maintain the scalar quantity, or how predictive the scalar quantity is of future values. The autocorrelation function for an individual particle is

$$R_i(\tau) = \frac{\overline{(U_i(t) - \overline{U}_i) \cdot (U_i(t + \tau) - \overline{U}_i)}}{\sigma_i^2}, \qquad (6)$$

where the bar denotes the mean particle position. The autocorrelation time

$$T_{AC} = \int \overline{R}_i(\tau) \qquad (7)$$

is the total time that particles retain memory of their initial values. High autocorrelation values indicate that a quantity is conserved.

3 Data from the PREDICT Experiment

3.1 Analysis data

The data used for this study from the PREDICT experiment is taken from the ECMWF model, which outputs velocity and moisture data on an evenly spaced planar grid with a

spatial resolution of 0.25 degrees and temporal output every 12 hours. Vertical levels for velocity data output are on constant pressure levels. In this study, the ECMWF model output and forecast data for the case of two developing storms from August 28 to September 17 is used, during the times that Gaston and Karl were tracked. Gaston had a visible pouch on Aug. 28, and was designated a tropical storm by National Hurricane Center forecasters on Aug 30 and was later downgraded on Sept. 2. The Ex-Gaston was trackable until Sept. 11, but never redeveloped. Karl had a well-defined surface low along the wave trough and associated pouch on Sept 9, and lasted until Sept. 17. Further details on the evolution of these storms is given in Montgomery et al. (2011), while the Lagrangian behaviour of these storms is described in Section 4.

The temporal output of forecast data is every 12 hours, with a 120 hour forecast run each day. The use of Lagrangian methods in analysing forecast data would reveal LCSs that would exist under the given forecast. The forecast data provides a way to compute repelling LCSs in real time, but will be addressed in a future study. For this study, we use only the available output data at 0 hours and 12 hours each day.

This study focuses on the kinematic aspects of genesis, which when combined with the dynamic and thermodynamic aspects, see Smith and Montgomery (2011), will help provide a more complete picture of genesis in the real atmosphere. For the kinematic boundaries, we focus on the model analysis data which incorporates dropsonde data, but we do not use dropsonde data directly since the Lagrangian computations require trajectory integrations which are far simpler using the model output grids.

3.2 Trajectory computations

All of the Lagrangian fields are computed daily for the entire domain by seeding particles at 0.125 degree intervals and computing particle trajectories both forward and backward in time. The time interval for model data is 12 hours, but we use a 1 hour intermediate time step on a fourth order Runge-Kutta solver to better resolve trajectory curvature. Interpolation of velocities is done by a simple feature tracking scheme which advects velocities from model output times to intermediate times by advancing the feature at the mean-flow speed. Linear interpolation in both time and space is then used to obtain fluid velocities. Since we use only velocity information available at the time and not forecast data to produce real-time Lagrangian fields, we primarily use a backward-time integration of trajectories, which requires velocity data at previous times. In order to balance the constraints of resolution, availability of information, and computational expense, we have chosen 48 hours as the integration time. This time is long enough to resolve individual LCSs while maintaining coherence of LCS's across varying initial times. Shorter integration times did not resolve LCS's as well, while much longer integration times resolved LCSs but were computa-

tionally expensive and sometimes yielded spurious structures associated with the domain boundary. Due to their objective nature, Lagrangian fields require 48 hours of velocities, but only require the computed pouch location as a point of reference for visualization at the initial time of integration. As discussed in Section 1.7, we have assumed that the flow is layer-wise 2D, and have chosen 500 hPa, 600 hPa, 700 hPa, 850 hPa, and 925 hPa as vertical levels for all computations.

Vorticity and OW values require the computation of velocity gradients, which are computed through second-order finite differences.

3.3 Simplifications used during PREDICT

During the PREDICT experiment, for each model output time, a pouch translation speed was computed to view the Lagrangian reference frame, assuming that the flow was steady in the moving frame and layerwise two-dimensional. To apply finite-time Lagrangian methods, the assumptions of a steady flow is unnecessary and Lagrangian structures are found independent of a computed translation speed. However, a layerwise two-dimensional flow is still assumed for simplicity and since convective features are not well resolved by global models[2].

Translation speed

Recirculation is the primary characteristic of a vortex which enables repeated moistening and vorticity amplification, and is generally not sensitive to small variations in the computed pouch translation speed. However, the flow boundaries outside the recirculation region directly impact which environmental air masses interact with the vortex and may be sensitive to variations in the translation speed. Differences in velocity between the inner-core circulation and the hyperbolic fixed point location or time variation in translation speed may cause drastic changes in the manifold structure.

Layerwise 2d flow

The assumption of a layerwise 2D flow is an appropriate simplification for describing differences between the steady and time-dependent flows. Even though trajectory motion is three-dimensional in regions of intense vortical convection, three-dimensional motions are not well resolved by the global models. Justification for computing two-dimensional structures on horizontal layers in a three-dimensional flow is provided by Rutherford et al. (2010), which showed that the two-dimensional projection of LCSs computed from three-dimensional trajectories were aligned across vertical levels

---

[2]The layerwise approximation is not strictly necessary since the Lagrangian methods have been recently established for three-dimensional flows (Haller , 2011; Rutherford and Dangelmayr , 2010). An analysis of the three-dimensional flow in the global models and observations will be conducted in due course.

up to 7 km in the vicinity of rotating deep convective structures [termed vortical hot towers (VHTs)]; the flow geometry was nearly two-dimensional even though trajectory paths were not. A similar alignment of LCSs across vertical levels is shown in this study though VHTs are not resolved. Although the Lagrangian methods can be developed for three-dimensional flows, the layer-wise two-dimensional assumption is a convenient simplification for the interpretation and computation of kinematic boundaries. The interpretation of boundaries is easier also in two dimensions since the manifolds are one-dimensional. Computations are simpler due to the larger data sets associated with three-dimensional velocity fields. Since we use a trajectory-based approach, the "vertical escape" of trajectories off of the horizontal slices is a concern of the simplification. While trajectories may escape, the persistence of coherent structures across vertical levels suggests that the flow geometry remains approximately planar even though trajectory motions may not.

Steady flow

While the layer-wise two-dimensional flow assumption is made with caution, we show that the assumption of a steady flow even in the translated Lagrangian frame of reference may sometimes yield undesirable results. The assumption of a steady flow may differ from the Lagrangian view if the time-variation is non-trivial. The translated Lagrangian reference frame, or the frame of reference moving with the mean flow speed (here the computed pouch translation speed), still assumes a nearly steady flow in that reference frame, and is only translation invariant. In contrast, the objective Lagrangian frame is Galilean invariant, which makes it invariant also under rotations and requires no knowledge of translation speed.

4 An analysis of time-dependence in tropical disturbances

In this section, we examine the kinematic structures which form finite-time boundaries and control particle transport between the environment and the pouch. Examples of these boundaries will be shown for ex-Gaston and pre-Karl before either was declared a tropical storm. The general results from utilizing a Lagrangian reference frame can be summarized as follows

1. Objective Lagrangian boundaries are sometimes different than streamlines in the moving frame with the wave translation speed.

2. The Lagrangian frame is shown to be more precise in diagnosing transport by a backward trajectory analysis

3. The Lagrangian boundaries are located relatively easily in real-time data

4. The LCSs form boundaries between air masses with high and low relative humidity and humidity

Particular results from the Lagrangian reference frame pertinent to developing and non-developing disturbances include

1. A pathway to the ITCZ is persistent for the developing case, but constricts for the non-developing case.

2. The vertical coherence of the pouch boundary is significantly degraded for the non-developing case. The pouch boundary becomes tilted and the upper-level boundary becomes irreversibly detached due to impinging vertical shear.

Reference frames

A commonly used reference frame in tropical meteorology is the Eulerian frame, in which streamlines are plotted in a ground relative frame of reference. In this reference frame, a passing Easterly wave represents a time-dependent flow, in which trajectories may cross Eulerian streamlines. Moreover, an Easterly wave does not generally have recirculating Eulerian streamlines prior to genesis, but does show recirculation as genesis is declared. For these reasons, this frame is suboptimal for diagnosing the true Lagrangian circulation of the flow. An improvement to this frame can be made by considering the speed of the translating wave. By subtracting the pouch translation speed, closed streamlines can be seen in pre-genesis disturbances, and particles are better constrained by streamlines in this moving frame. We refer to this reference frame as the translated Lagrangian reference frame. In this frame, a clearer view of the geometry associated with recirculation can be seen by a saddle point often appearing outside of the pouch, and stable and unstable manifolds forming the pouch boundary, Figure 1. The unstable manifold encloses the pouch. Figure 2 (a) shows the translated Lagrangian streamlines, along with trajectory locations which enter a circle of 3 degree radius around the pouch center within 48 hours at the same time as the streamlines. Some particles that enter the pouch from the northeast not only cross Eulerian streamlines but also cross the translated Lagrangian streamlines. The lesson learned from this example is that even Lagrangian streamlines are not impermeable to particle transport through the time-varying flow.

Sensitivity to changes in translation speed

Time-variations and spatial variations of the pouch translation speed may alter the streamline structure in the translated Lagrangian frame. The time variation of the computed pouch translation speed over a 12 hours time interval at times exceeds $2\ ms^{-1}$. Spatial variations in velocities between a pouch center and pouch boundary also often exceed $2\ ms^{-1}$.

The effect of a $2\ ms^{-1}$ change in translation speed is shown in Figure 2 (a, b) along with the locations of particles which are within 3 degrees of the pouch center within

(c)
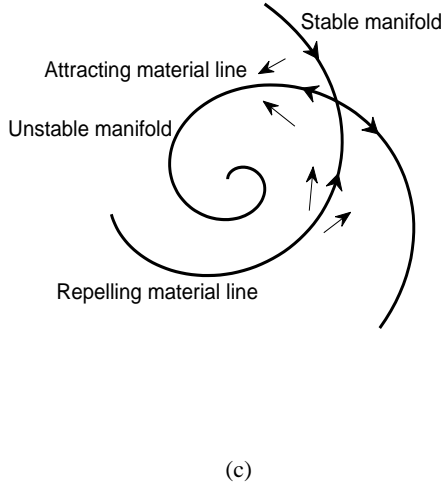
Fig. 1. Schematic of the hyperbolic fixed point and manifolds near a convergent vortex.

48 hours. There are saddle points to the northeast and west of the storm, and the northeast saddle point and associated streamlines constrains the movement of the particles to the north. The streamlines with the computed translation speed indicate that the particles to the north will move south toward the storm, but will be taken to the east as they move southward, and will not enter the storm. Streamlines computed with the higher translation speed show that the saddle point is now located to the east of the storm. The streamlines indicate that the particles from the north will now pass to the west of the storm without entering the pouch. The particles' final locations are mistaken by the streamlines computed from either translation speed, where in fact, the particles enter the pouch. Since the particles originate from a region with low relative humidity, the streamlines underestimate the amount of dry air entering the pouch. The differences in translation speed tend to have less effect on the geometry of strong vortices (Riemer and Montgomery , 2011).

Since the Lagrangian frame does not require a translation speed, it is not sensitive to variations in translation speed.

LCSs

It is not possible to compute streamlines in the Lagrangian frame for a time-dependent flow. However, LCSs are the finite-time approximations to stable and unstable manifolds of a hyperbolic fixed point. In Figure 2 (c), the backward time FTLE field for ex-Gaston at 850 hPa has a prominent LCS which is in nearly the same location as the unstable manifold in the translated Lagrangian frame, but the LCS is not crossed by particle trajectories. To reach the pouch cen-

ter, trajectories travel around the LCS, which allows the set of trajectories from the northeast to enter the core. The LCS wraps around the core, allowing a recirculation region inside the LCS. The forward time FTLE field, Figure 2 (d), shows only a weakly repelling LCS where the stable manifold resides, which implies that particle transport into the vortex is primarily determined by the attracting LCS.

Differences in the LCSs and streamlines away from the hyperbolic fixed point are due to the time-variation in velocities. However, if the velocity near a stagnation point is slow, the manifolds may be computed while the LCS associated with the manifold does not exist, since there is not sufficient particle separation. The nonexistence of an LCS where a stable manifold resides provides an explanation to how particles appear to pass through the manifold. By inverting the FTLE value, the time scale of LCSs can be defined as the time required for a factor of e separation.

FTLE values along repelling LCSs during periods of convergence are often smaller than the FTLE values along the attracting LCS. When the FTLE values show a time scale near 12 hours, or on the order of the autocorrelation time of fluid velocities, the LCSs tend to be well resolved and persistent across varying initial time. However, LCSs with smaller FTLE values and time scales near the integration time of 48 hours are not well resolved and do not persist across varying initial times. In this case, since particles lose memory of their velocities far sooner than the typical separation time of trajectories, the separation of particles is due to the time change of velocities, and is not related to a strong flow feature.

If attracting and repelling LCSs are resolved, transport across the Eulerian manifold is still possible through lobe dynamics. Enclosed lobes formed from intersecting sections of LCSs allow material to enter the circulation center through the deformation of the LCSs even when the LCSs are persistent.

The foregoing considerations offer two explanations as to why the particles pass through the stable manifold to bring dry air to the circulation center.

Time-variation and autocorrelations

While streamlines and saddle-point locations are sensitive to time-dependence of velocities. LCSs are not subject to this sensitivity. Moreover, LCSs tend to be material lines. Particles which remain on an LCS tend to preserve maximal Lagrangian quantities, while they do not preserve Eulerian quantities. Preservation of maximal Lagrangian values can be seen by viewing the attracting and repelling FTLE-fields for pre-Karl from September 11 in Figure 3 (a,b) and the fields in Figure 3 (c,d). The major LCSs are trackable as they move with the disturbance over 2 days. Eulerian quantities, e.g. vorticity and OW shown in Figure 3 (e,f), are not well conserved, particularly in regions of high strain. The straining regions marked by negative OW values occur mainly outside the circulation center and are generally in the same re-
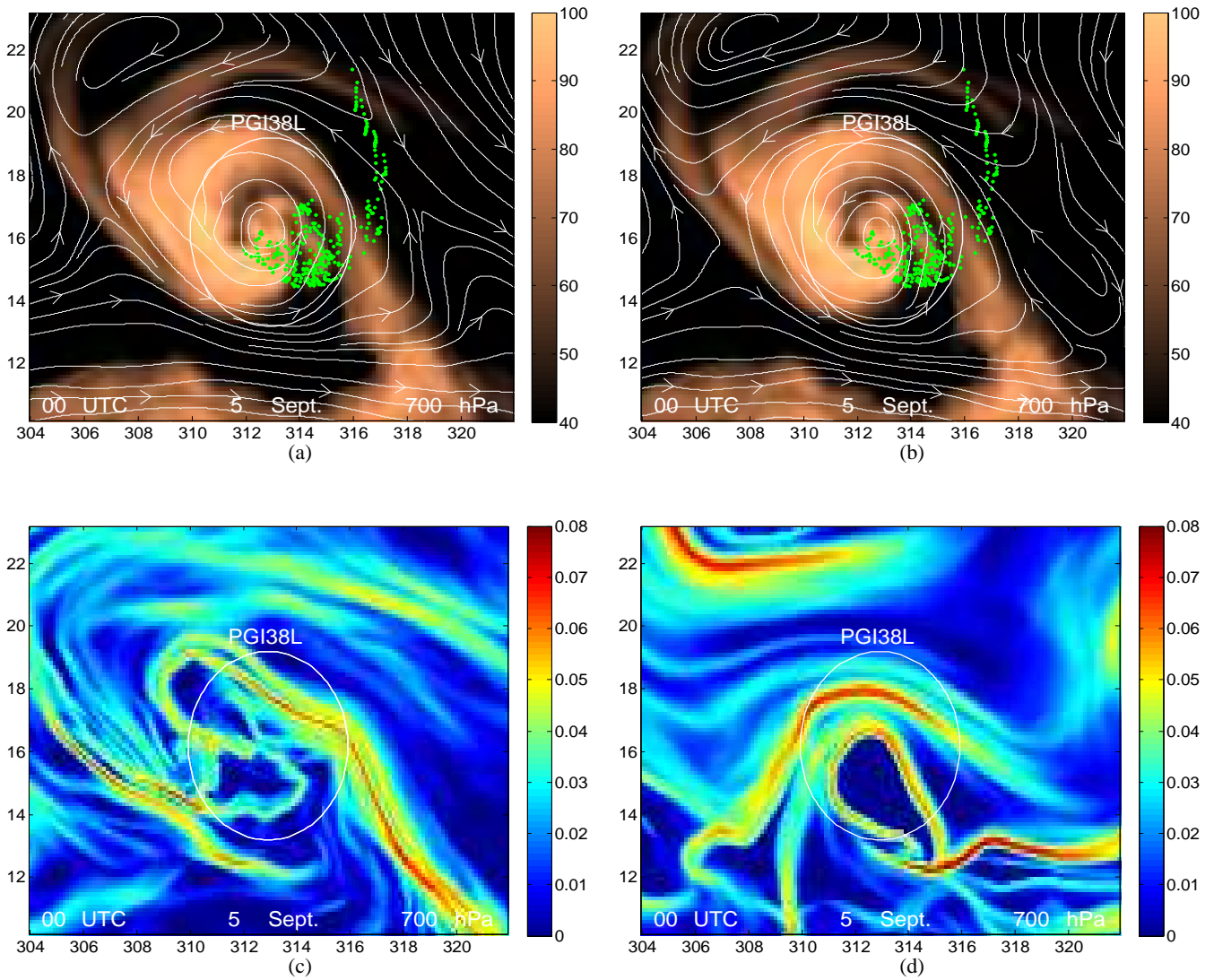
Fig. 2. Relative humidity field with streamlines in comoving frame (a) and comoving frame with $2\ ms^{-1}$ variation in translation speed (b) shown on Sept. 5 for ex-Gaston with particle locations beginning in the pouch on Sept. 7. Backward time (c) and forward time (d) FTLE fields are shown on Sept. 5.
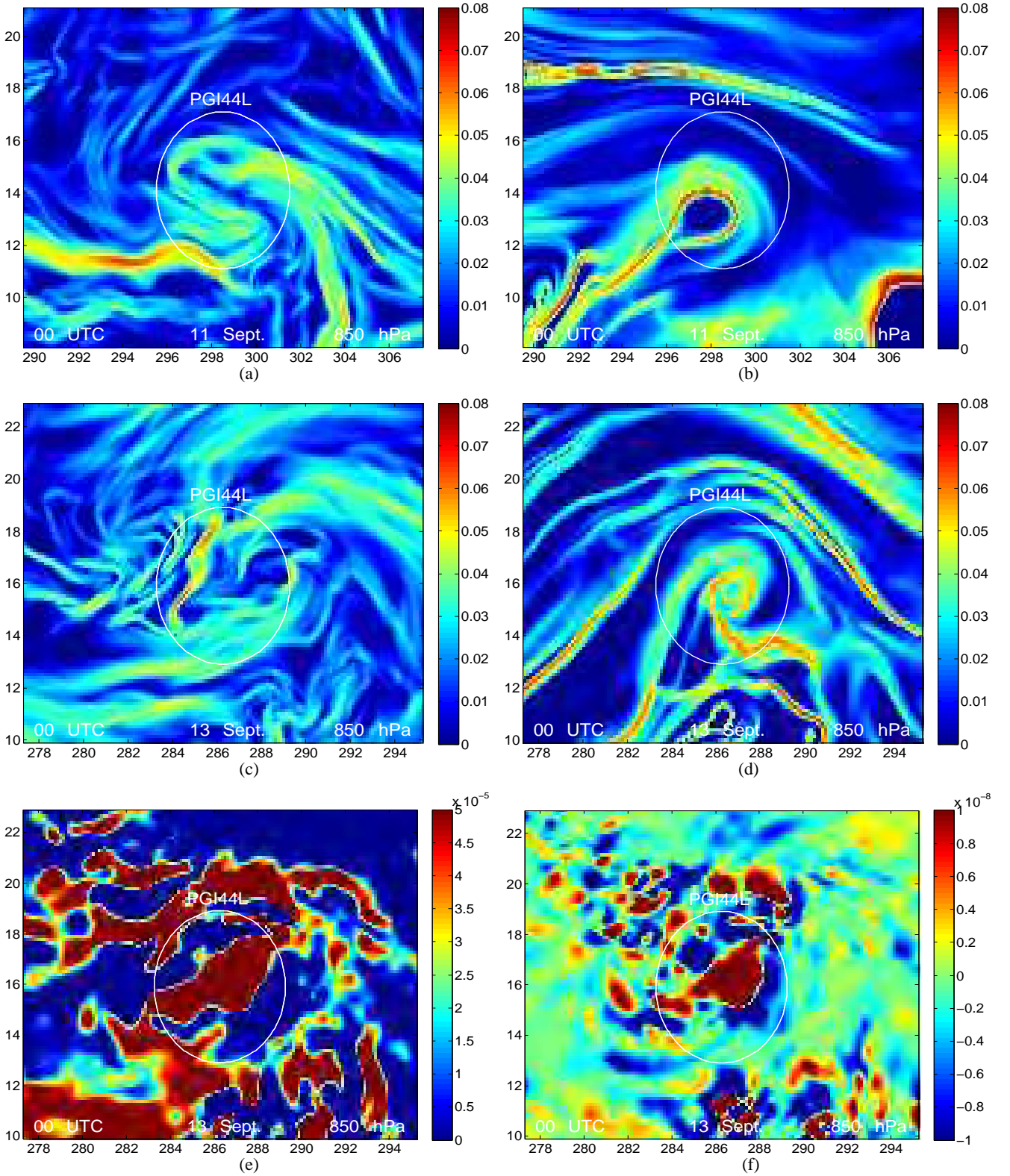
Fig. 3. The backward and forward time FTLE fields are shown for Sept 11 at 850 hPa in (a) and (b) for pre-Karl. The backward and forward time FTLE fields for Sept. 13 are shown in (c) and (d). Vorticity and OW are shown at the same time in (e) and (f) respectively.

gions where the LCSs exist, though the detail shown by the LCSs is far greater.

The time variation of quantities along particle trajectories can be further quantified by the memory of Lagrangian and Eulerian quantities through the integrated autocorrelation function, see eqs. 7 and 8, along a set of backward trajectories initiated at the pouch center. Autocorrelation have been computed for particle speeds, relative humidity, the OW parameter, and vorticity. The autocorrelation times indicate that while fluid velocities are retained along particle trajectories for at most 12 hours, vorticity an OW are conserved for less than 6 hours. However, the Lagrangian fields have autocorrelation times between 18 and 36 hours and carry more memory of their previous values than any of the Eulerian fields derived from fluid velocities. Relative humidity has autocorrelation times of up to 24 hours, and used as a two-dimensional tracer is an indicator of the original moisture content of particles entering the pouch.

Flow boundaries and tracer fields

The relation between LCSs and particle trajectories can be seen further by comparing the Lagrangian fields to a tracer field. The attracting LCSs are shown for ex-Gaston in Figure 4 (a) on Sept 4 with relative humidity values on the same day shown with particles that will enter within a 3 degree radius of the pouch in Figure 4 (b). The repelling LCS is shown for comparison in Figure 4 (c). Relative humidity in the Lagrangian frame is used as a tracer field (by advecting the field forward in time and pretending there are no sources or sinks) in Figure 4 (d), which shows the relative humidity values on Sept 2 at particle locations on Sept 4. There are strong similarities between the tracer field and the attracting structures on Sept 4 shown in Figure 4 (e). The alignment of tracer gradients with LCSs (whose orientations are closely related to strain eigenvectors) is a more general result of Lapeyre et al. (1999). In contrast, the relative humidity analysis data shown on Sept 4 in Figure 4 does not provide much information about the transport of particles. A similar scenario can be seen for pre-Karl in Figure 5.

Vertical Structure

Vertical alignment of LCSs is required for the LCSs to act as flow boundaries, so that they form a two-dimensional manifold in the three-dimensional flow. In Figure 6, the FTLE ridges are overlaid on relative humidity fields for ex-Gaston and pre-Karl at levels of 500 hPa, 700 hPa, and 925 hPa . The pouch boundary of ex-Gaston is displaced and rotated between vertical levels, while pre-Karl has far greater vertical coherence. For both storms, the manifolds associated with the saddle to the west of the pouch do not coincide with LCSs at multiple vertical levels.

5   Analysis of a non-developing and developing disturbance

We now apply the Lagrangian methods to the cases of Gaston and Karl to show what additional insight these methods can provide in the development or non-development of a tropical depression.
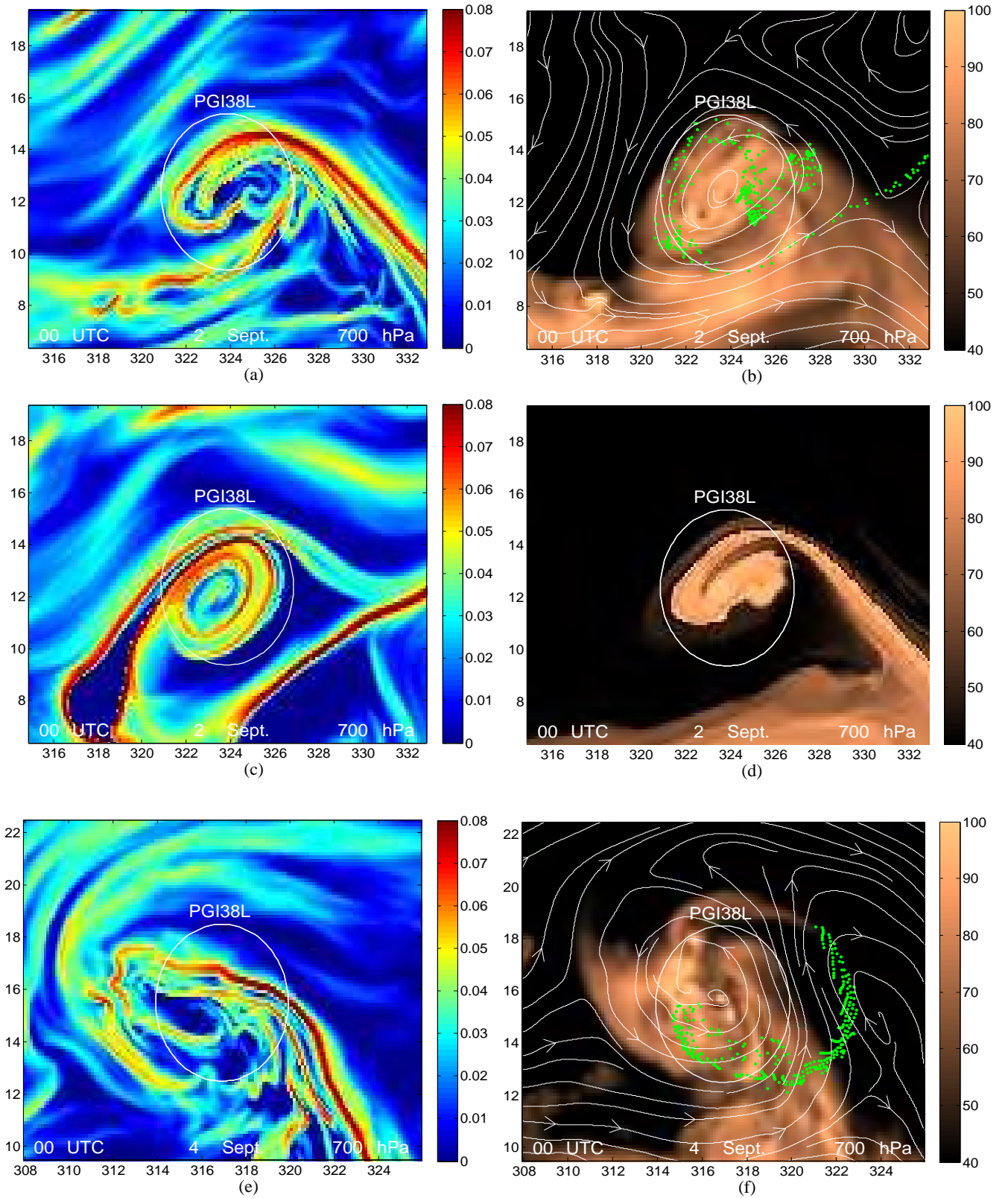
5.1   Evolution of ex-Gaston

5.1.1   Summary

To provide insight as to why ex-Gaston did not re-develop, we look at the potential intrusion of dry air into the storm at 700 hPa and above which caused the pouch to become shallower. Gaston was declared a tropical storm on Sept. 1 but was downgraded to a tropical depression on Sept. 2. Gaston resided in a relatively moist environment with high moisture at lower levels but surrounded by dry air at upper levels. The influence of the dry air can be seen by deep shear and pouch shear above 12 ms^{-1} prior to Sept. 1, and approximately 8 ms^{-1} beginning on Sept. 1. The dry air had penetrated the pouch at mid and upper levels by Sept 5. Before Sept. 5, this intrusion was not noticeable at 700 hPa, and lower levels actually showed moistening (Montgomery et al. , 2011). The interaction of dry air with the pouch suggests that the pouch was subjected to vertical wind shear (Davis and Ahijevych , 2011). Smith and Montgomery (2011) show that the dry air entering the pouch decreased θ_e in the mid to lower troposphere but did not produce downdrafts strong enough to decrease the boundary layer θ_e. On Sept 1, the pouch has high relative humidity at 700 hPa, but is surrounded by dry air. The relative humidity profile at 700 hPa did not show significant change before Sept. 5, with more dry air entering on Sept. 6. The Lagrangian coherent structures and trajectory analysis, as well as a tracer field, will demonstrate that the intrusion of dry air was occurring prior to Sept 5, but the air was presumably moistened from convection. However the pouch structure was significantly degraded. Sept 5 marked the point where the intrusion of dry air and escape of moisture through ventilation could not be overcome by convective moistening from below. By this point, the pouch had already lost all vertical structure. A time series of pouch averaged relative humidity, vorticity and OW are shown in Figure 7. Time series showing the evolution of forward and backward time Lagrangian quantities are shown in Figures 8 and 9.

5.1.2   Lagrangian analysis

The evolution of the Lagrangian fields at 700 hPa is shown for Sept 1 through Sept 6 in Figure 10. The primary attracting LCS at 700 hPa, where the intrusion of dry air is noticeable, has a tail southeast of the pouch and wraps cyclonically around the north side of the pouch. A repelling LCS intersects the attracting LCS at the northern edge of the pouch and forms a wavelike boundary which prohibits the interaction of

Fig. 4. The evolution of LCSs can be seen for Gaston in the backward time FTLE field (a), relative humidity field (b) and forward time FTLE field (c) on Sept 2 and the Lagrangian relative humidity field shown with relative humidity values on Sept 2 at particle locations on Sept 4 (d). The backward time FTLE field (e) and relative humidity field (f) are shown on Sept 4.
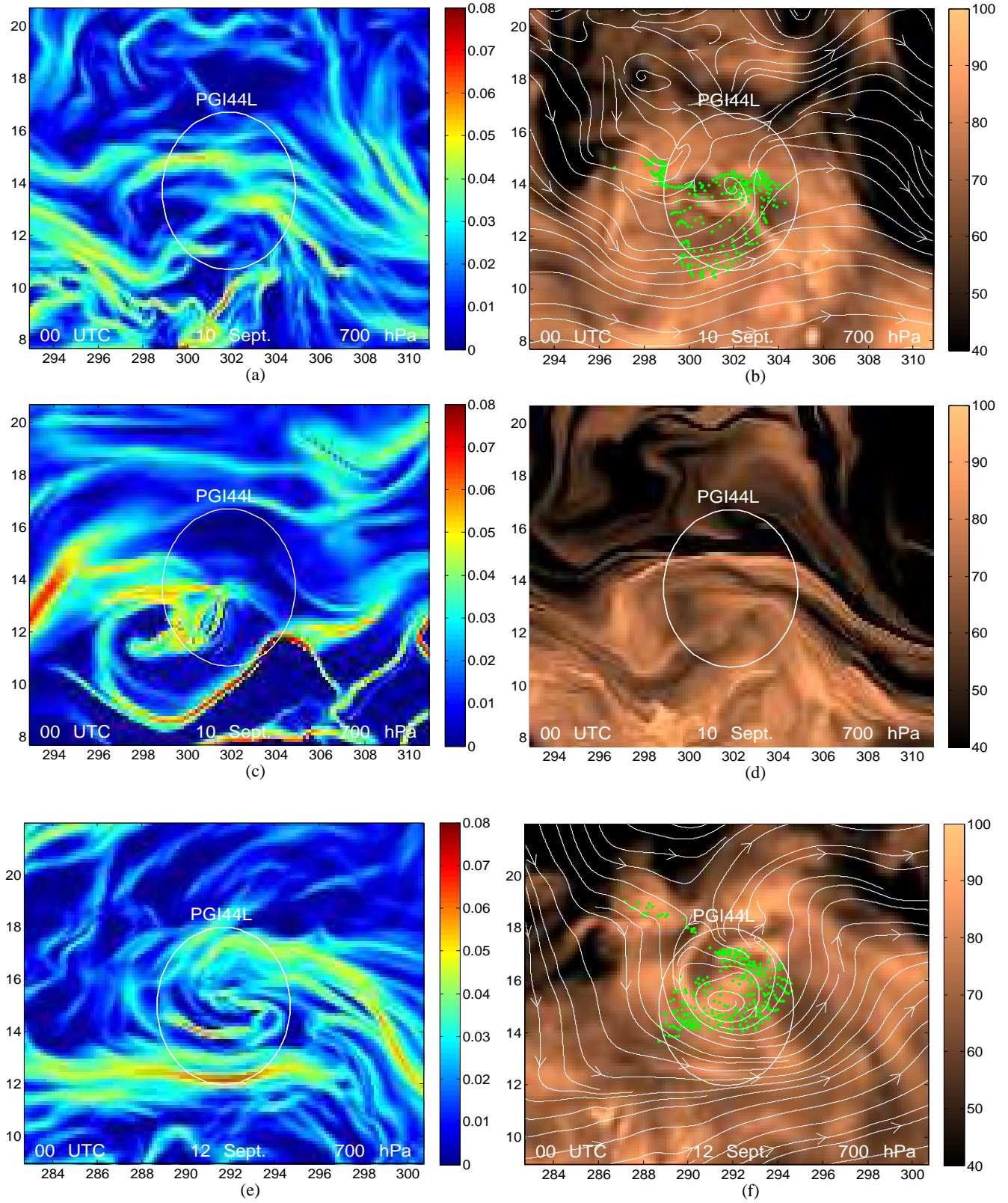
Fig. 5. The evolution of LCSs can be seen for pre-Karl in the backward time FTLE field (a), relative humidity field (b) and forward time FTLE field (c) on Sept 10 and the Lagrangian relative humidity field shown with relative humidity values on Sept 10 at particle locations on Sept 12 (d). The backward time FTLE field (e) and relative humidity field (f) are shown on Sept 12.
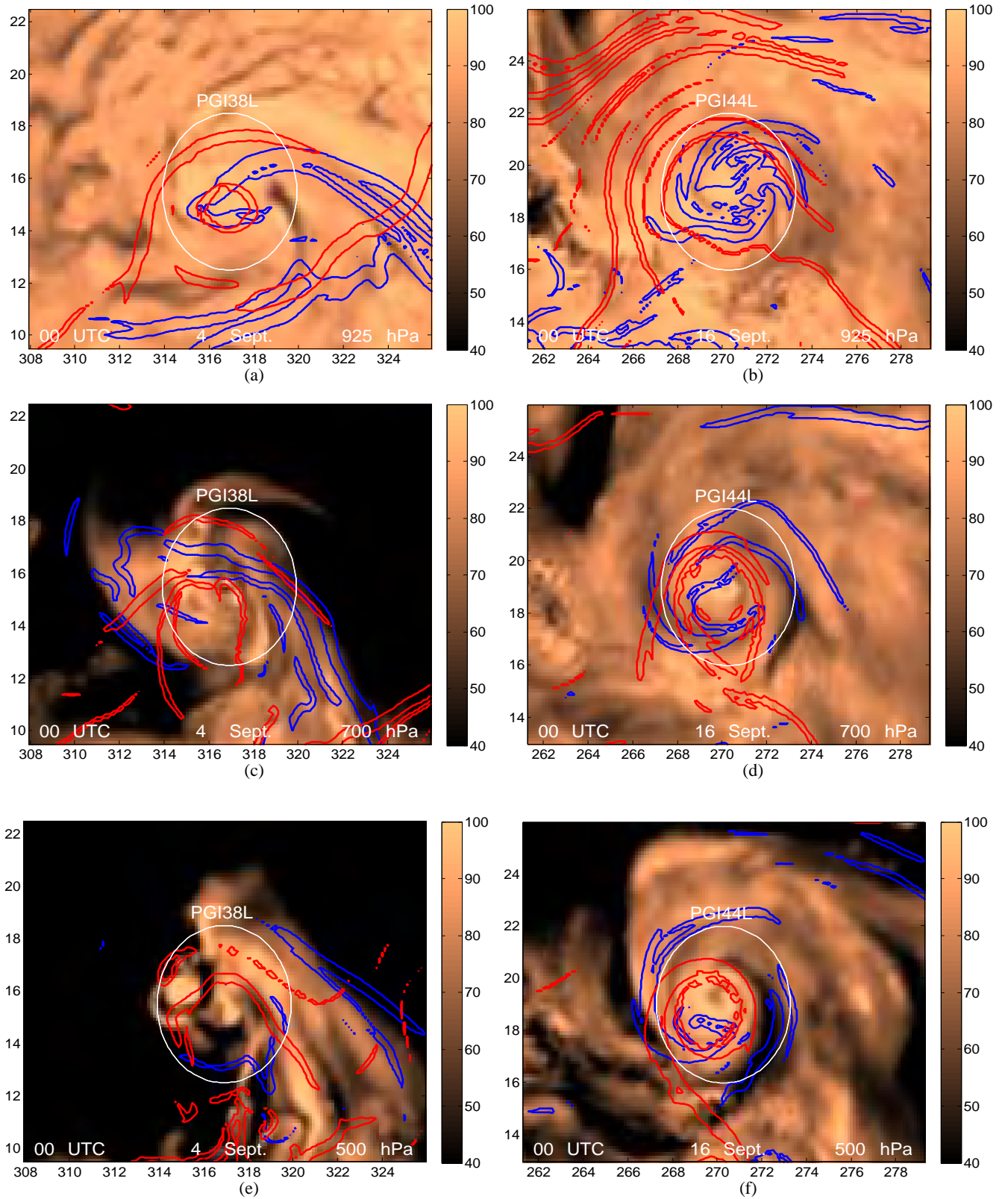
Fig. 6. Attracting LCSs (blue) and repelling LCSs (red) are overlaid on the relative humidity field for ex-Gaston on Sept 4 at levels of 925 hPa, 700 hPa, and 500 hPa in (a), (c), and (e), and for pre Karl on the same levels in (b), (d), and (f).
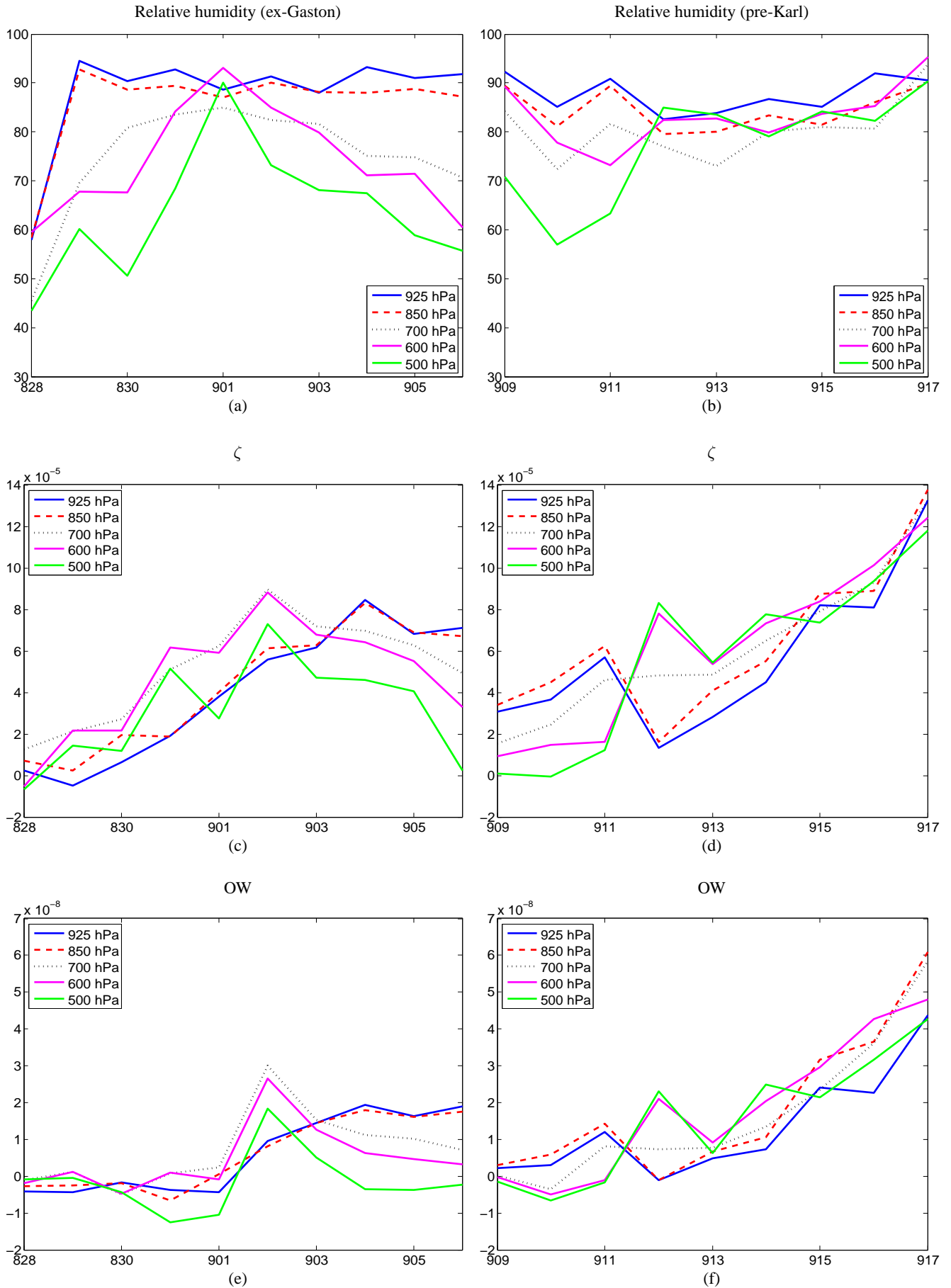
Fig. 7. Pouch averages of Eulerian quantities for the 2 degree circle surrounding the pouch are shown for ex-Gaston (left) and pre-Karl (right) for the relative humidity (a, b), ζ (c, d), and Okubo-Weiss parameter (e, f). The different curves represent vertical levels of 500 hPa, 600 hPa, 700 hPa, 850 hPa, and 925 hPa.
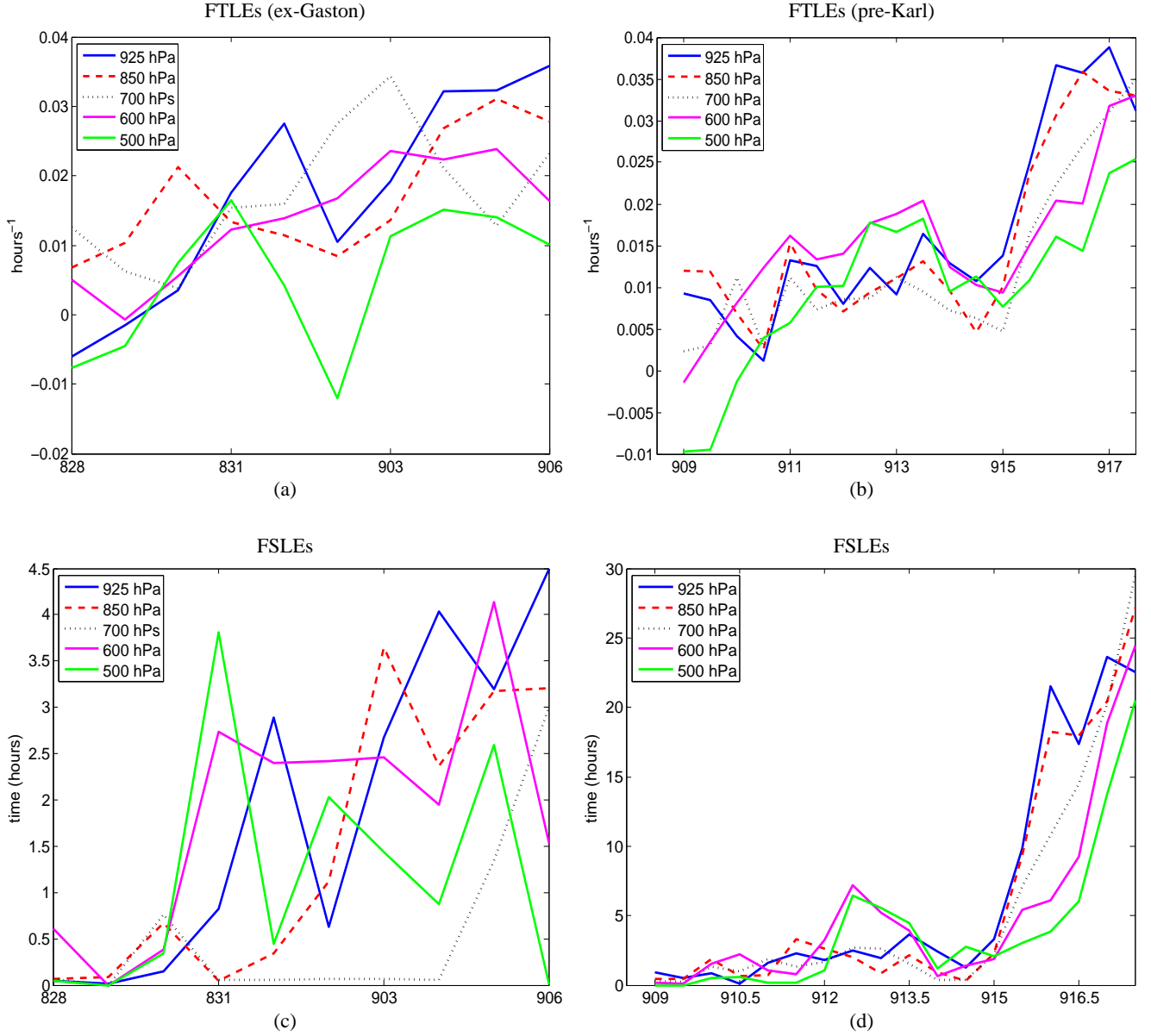
Fig. 8. Pouch averages of backward-time Lagrangian quantities for a 2 degree circle surrounding the pouch are shown for Gaston (a,c) and Karl (b,d) for the FTLEs (a,b), FSLEs (c,d). The different curves represent vertical levels of 500 hPa, 600 hPa, 700 hPa, 850 hPa, and 925 hPa.
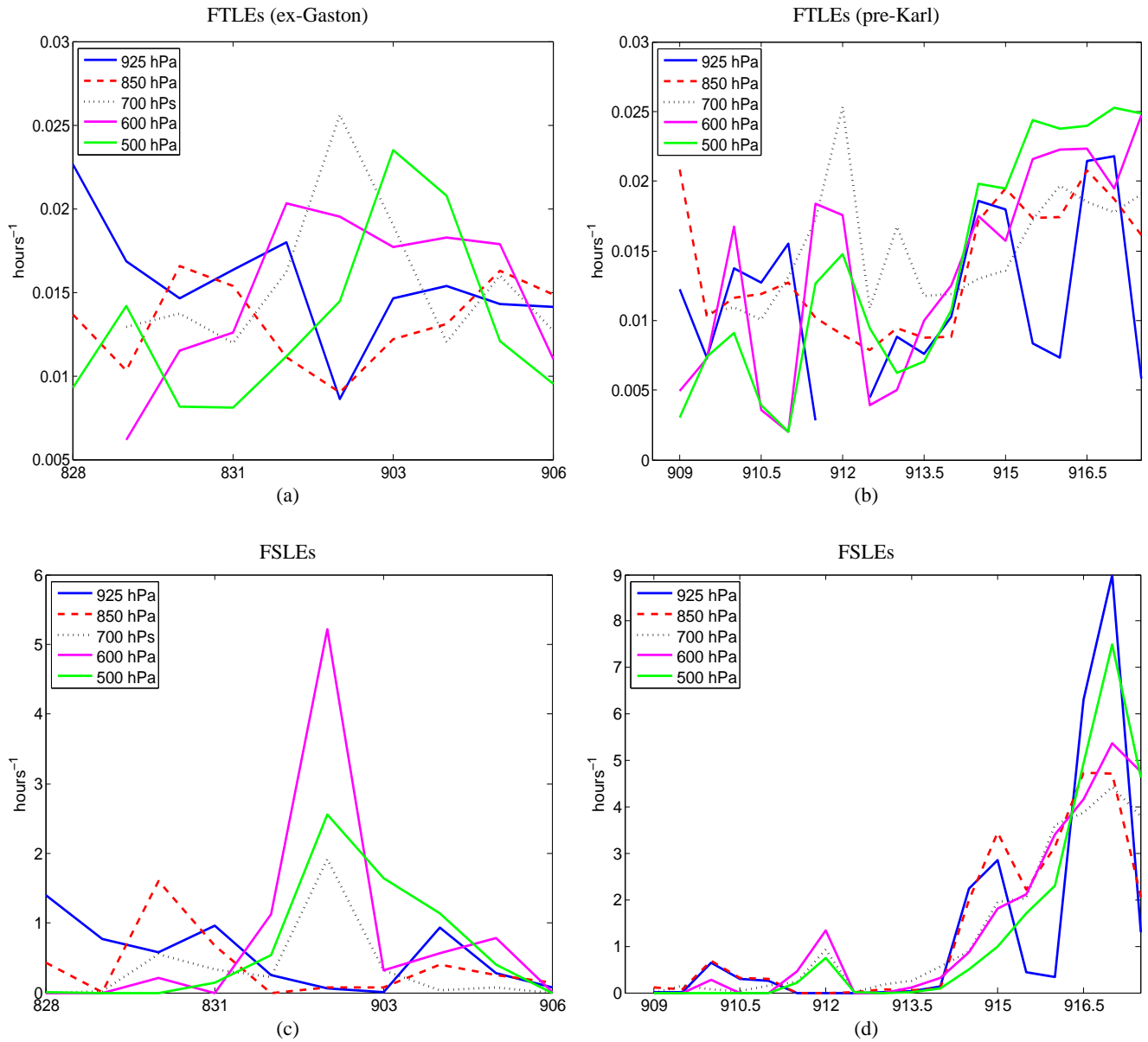
Fig. 9. Pouch averages of forward-time Lagrangian quantities for a 2 degree circle surrounding the pouch are shown for Gaston (a,c) and Karl (b,d) for the FTLEs (a,b), FSLEs (c,d). The different curves represent vertical levels of 500 hPa, 600 hPa, 700 hPa, 850 hPa, and 925 hPa.

the pouch and air masses to the north, very similar to the cat's eye streamlines. This boundary is approximately located on the boundary between the moist air in the pouch and the dry air to the north and east of the pouch and containing moist air at 700 hPa, Figure 10 (a). The attracting LCS forms most of the boundary to the north, and resides approximately 3 degrees from the pouch center. The attracting LCS forces air that is east of the structure to wrap around the pouch, and the air does not enter for at least two days.

Vertical wind shear pushes particles from a broad region of low relative humidity to the north toward the pouch (Davis and Ahijevych , 2011), and forces the LCS southward. These particles do not directly enter the pouch as they are blocked by the attracting LCS, which forces the particles to wrap around the west side of the pouch. By Sept. 2, the attracting LCS splits east of the pouch center, begins to effectively "unzip", Figure 10 (b), and part of the LCS begins to travel cyclonically around the center. This branch rejoins the stationary branch on Sept. 4 after making one revolution around the pouch, Figure 10 (c-e). During the revolution, this branch allows inward transport of dry air through lobe dynamics as the repelling LCS is distorted. As the repelling LCS vanishes between Sept. 3 and Sept. 4, a pathway opens for the direct import of dry air from the West. As it rejoins the first branch, it constricts the moisture source from the ITCZ to the south, Figure 11 (b-e).

A pathway for material exiting the pouch also emerges due to a change in the flow field and is marked by the presence of a repelling LCS, which appears at 700 hPa and above on Sept. 2. The aggregate contribution of the repelling LCS can be seen by the time series of forward time FTLE and FSLE values in the Figure 9, which shows higher Lagrangian values at 600 and 700 hPa beginning on Sept. 2 at the time where significant mixing was occurring in the pouch. Repelling LCSs at the pouch center normally have a time scales on the order of the integration time but this LCS has a time scale of far less, making it more important for transport. After the repelling LCS appears and the ITCZ moisture source is removed, air from the pouch is allowed to leave the pouch to the west.

The relative humidity tracer field, at 700 hPa in Figure 11 and 500 hPa in Figure 12, shows the initial moisture content of air parcels entering the pouch and confirms that some of the air entering the pouch is initially dry while the air exiting the pouch is initially moist. The relative humidity tracer field indicates that dry air is already entering laterally, Figure 11 (a). The dry air was entering prior to Sept. 2, before the repelling LCS had completely formed the boundary. From Sept. 2 to Sept. 4, mostly moist air remains at the circulation center, but some dry air passes to the center through lobe dynamics. By Sept. 3, the relative humidity tracer field with relative humidity values from Sept. 1 shows an intrusion of dry air in the pouch which entered from the southwest along the second LCS branch. By Sept 4, the air from the north has forced the LCS southward and deformed the portion of the

repelling LCS wrapping around the west side of the pouch so that the dry air intrusion can enter the pouch directly. A comparison of the relative humidity tracer field to the FTLE field on Sept 3 reveals that the LCSs are aligned with the relative humidity gradient. The intrusion of moisture continues over the next 3 days, and by Sept 6, the relative humidity tracer field shows that initially dry air has entered the pouch while moist air has exited the pouch to the west. The expulsion of moist air seen in the relative humidity tracer field occurred at the same time that the repelling LCS emerged at the pouch center. This repelling LCS and the absence of an attracting LCS provides a mechanism for lobes of moist air to be expelled from the center to the west of the storm.

The time series showing approximately constant relative humidity until Sept. 4, Figure 7 implies that dry air entering the pouch occurs at 700 hPa and above and is compensated by convection and the associated vertical transport of moisture from below. This view is also supported by the study of the thermodynamics of ex-Gaston by Smith and Montgomery (2011). By Sept 6, the dry air intrusion diminishes the relative humidity profile in the pouch. Similar degradation of the pouch occurred above 700 hPa, Figure 7 while the low-level profile of the storm was still very favourable during this entire time period.

The vertical structure of Gaston is shown on Sept. 1 and Sept. 2 in Figure 13. A coherent boundary from 925 hPa to 700 hPa in the vicinity of the Eastern stagnation point is present on Sept. 1, but is absent above 700 hPa. After Sept 1, the attracting boundary is rotated and tilted, disrupting the vertical alignment of the pouch as the pouch boundary at 700 hPa and above is south of the boundary below 700 hPa. A tilted pouch makes it possible for dry air which has come from the north to enter the low level circulation from aloft. However, the two-dimensional trajectory analysis as well as the thermodynamic analysis of Smith and Montgomery (2011) suggest that the dry air is from the north. On Sept. 2 the already shallow pouch deteriorates further as the repelling LCS at 700 hPa near the stagnation point detaches from the LCSs below 700 hPa, and the attracting LCS at 700 hPa detaches from the LCSs below 700 hPa. The attracting LCSs at 700 hPa actually align orthogonal to those below 700 hPa. The repelling LCS on the West side of the pouch has also become stronger at this time and intersects the attracting LCS near the pouch center.

Further change in the vertical alignment on the pouch occurs from Sept 1 to Sept 5. While the pouch boundary remains in the same location relative to the pouch center below 700 hPa, the boundary moves southward at 700 hPa as particles from the north push the boundary southward. As the LCS is pushed southward, the circulation is tilted. The deformation of the pouch boundary in relation to particle trajectories and the pouch center in the moving frame can be seen in Figure 14. Trajectories which are in a 5 degree box around the pouch on Sept 4 are shown at times varying from Sept 1 to Sept 4 with LCSs at the same times at 700 hPa with

time increasing on the vertical axis. The Lagrangian pouch boundary at 700 hPa is tilted relative to the low-level center and rotated, which can be seen by a southward displacement as time increases.

Based on the foregoing results, the LCSs are implicated in the import of dry air, the vertical tilting of the vortex, a constriction of the ITCZ moisture source, and the expulsion of moist air when a repelling LCS is present. The repelling LCS is particularly important since it is the signature of a vortex which is turned inside-out, shifting from a period of net inflow to net outflow. The LCS view differs from the study of Schubert et al. (1999), which showed a vorticity profile that was radially inverted due to shear instabilities. Because the radial profile of vorticity is approximately monotonic, the profile does not support these instabilities. The thermodynamic implications of a dying vortex are important also, as the planar outflow limits the ability of convection to transport moisture upward. For a developing vortex, the amplification of vorticity occurs ultimately through vortex tube stretching associated with convection. However, the presence of a repelling LCS wrapping around the vortex core indicates that convective activity is diminished since the air which has been transported inward is now mixed or transported outward. In Rutherford et al. (2010), the presence of an repelling LCS marks the end of the convective lifecycle of a three-dimensional vortical hot tower. The splitting of attracting LCSs that enclose vortices has also been seen in dying vortices (O'Farrell and Dabiri , 2010).

5.2 Evolution of Karl

5.2.1 Summary

Karl was classified as a tropical disturbance on Sept 9, and had a trackable wave pouch. From Sept. 10 to Sept. 14, the near-surface circulation gradually increased in association with an approximate diurnal cycle of convective activity over the four day period of time before exhibiting a persistent region of central dense overcast on the day of development, Sept 14 (Montgomery et al. 2011). The progressive increase of circulation is shown in the time series of area-averaged vorticity within the pouch region at various vertical levels in Figure 7.

5.2.2 Lagrangian analysis

An analysis of the LCSs and their relation to moisture fields show that pre-Karl was far more favourable for development due to greater vertical alignment of the LCSs, and a more favourable location of LCSs relative to the pouch center. The absence of a repelling LCS enclosing the pouch center is also important since there is no pathway for particles to escape the pouch. The relative humidity tracer fields show that the particles entering the pouch are more moist than those entering Gaston.

The LCSs show less disruption from vertical wind shear than those from Gaston, which can be seen by noticing that the FTLE fields in Figures 6 show a region of convergence at the boundary between dry and moist air, which leads to the interaction of dry air with the pouch, while those of pre-Karl in Figures 15 and 16 show little influence from dry air regions. The relative humidity profile of pre-Karl at 500 hPa on Sept. 10 to Sept. 12 is very similar to ex-Gaston on Sept. 1, while it is more moist at 700 hPa. However, the LCS structure for Karl did not provide a pathway for dry air or isolate the storm from the ITCZ. On Sept. 13, the LCSs at both 500 hPa and 700 hPa formed a boundary to dryer air wrapping from the North side of the pouch and entering from the West. The lack of a secondary attracting LCS branch prohibits transport of dry air into the pouch through lobe dynamics.

The location of the LCS boundary to the north of Karl is different than for ex-Gaston. Karl has a wavelike boundary on the north side of the pouch but further North of the pouch center than ex-Gaston, Figure 15, with long LCSs along a broad line of sporadic convection(Smith and Montgomery , 2011), but little cyclonic rotation. The LCSs protect Karl from importing air from the North with relative humidity levels of below 60% from Sept 10 to Sept 12. These LCSs differ from the similar LCS seen in Gaston in that it does not split and unzip, which allows the ITCZ to remain a source of fuel. On Sept 12, the LCSs form an enclosure of a small region in the pouch center. In this region, convective activity can be seen in the forward time FTLE field by high isolated FTLE values (Rutherford et al. , 2010). By Sept 13, a dry air intrusion has wrapped from the north around the west side of the storm, and begins to enter from the southwest, but is far narrower than the dry air intrusion that entered ex-Gaston. A complete enclosure around the pouch, surrounding the entire 3 degree radius circle around the pouch center can be seen on Sept. 15, Figures 15 and 16. The LCSs are far North of the pouch even at 500 hPa, which keeps the dry air far from the pouch center. The LCS boundary is not forced Southward toward the pouch center by vertical wind shear, so the pouch maintains vertical alignment. The LCS structure and relative humidity tracer fields indicate that Karl was able to import additional moisture to compensate for the small intrusion of dry air. The dry air from this intrusion reaches the pouch center on Sept 16, but Karl had already developed. Karl is able to overcome the dry air since the intrusion does not remove the moisture source from ITCZ to the south, which can be seen in the relative humidity tracer fields, Figures 15 and 16.

The final locations of backward trajectories originating in a 3 degree circle around the pouch center indicate that they remain near the circulation center, Figure 5 (b, f), even 6 days before Karl was declared a tropical cyclone. The relative humidity tracer fields at 700 hPa and 500 hPa further demonstrate that the air entering the pouch center of Karl was moist from 700 hPa to 500 hPa, Figures 15, 16.
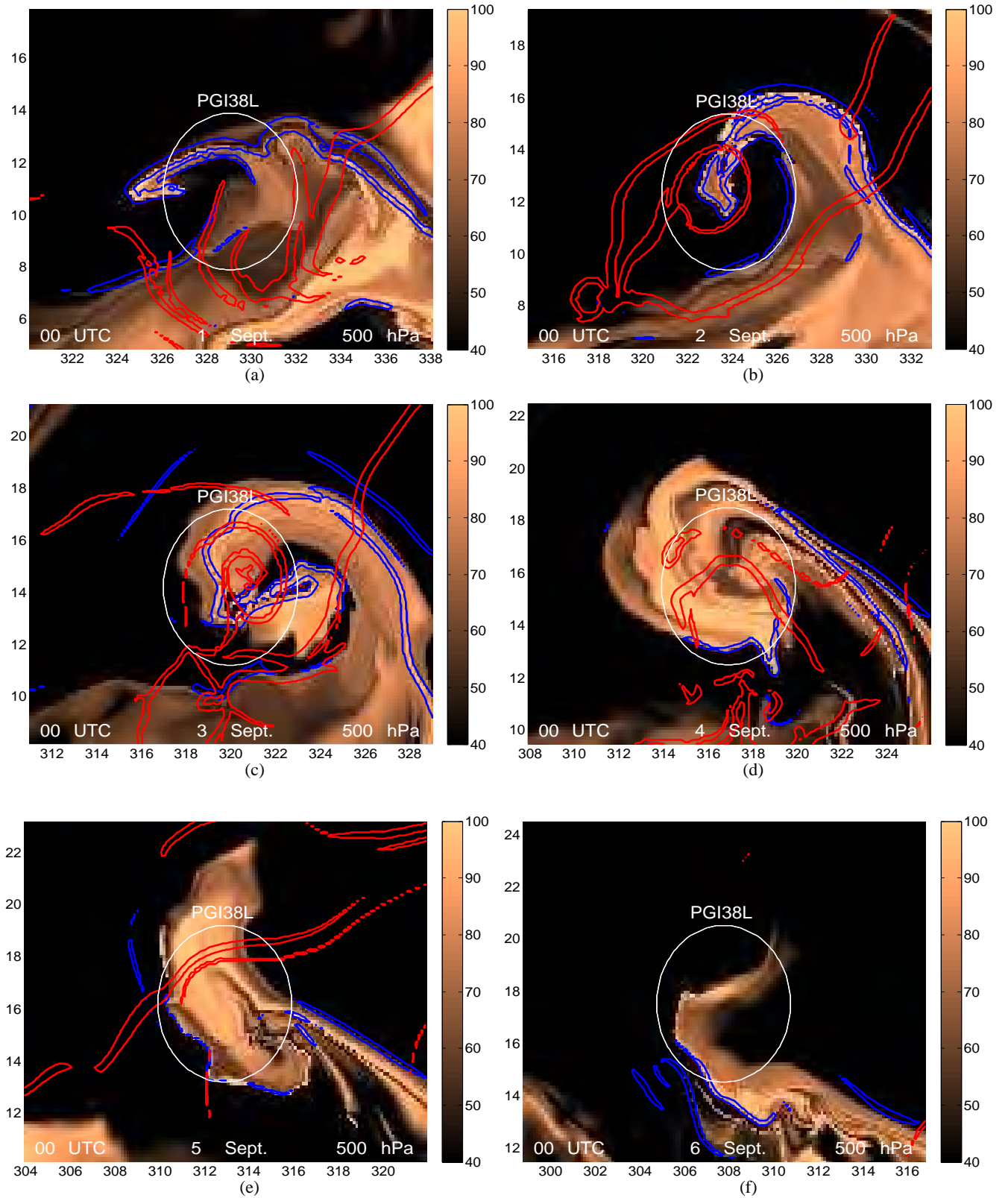
The aggregate contribution of LCSs is similar on all verti-
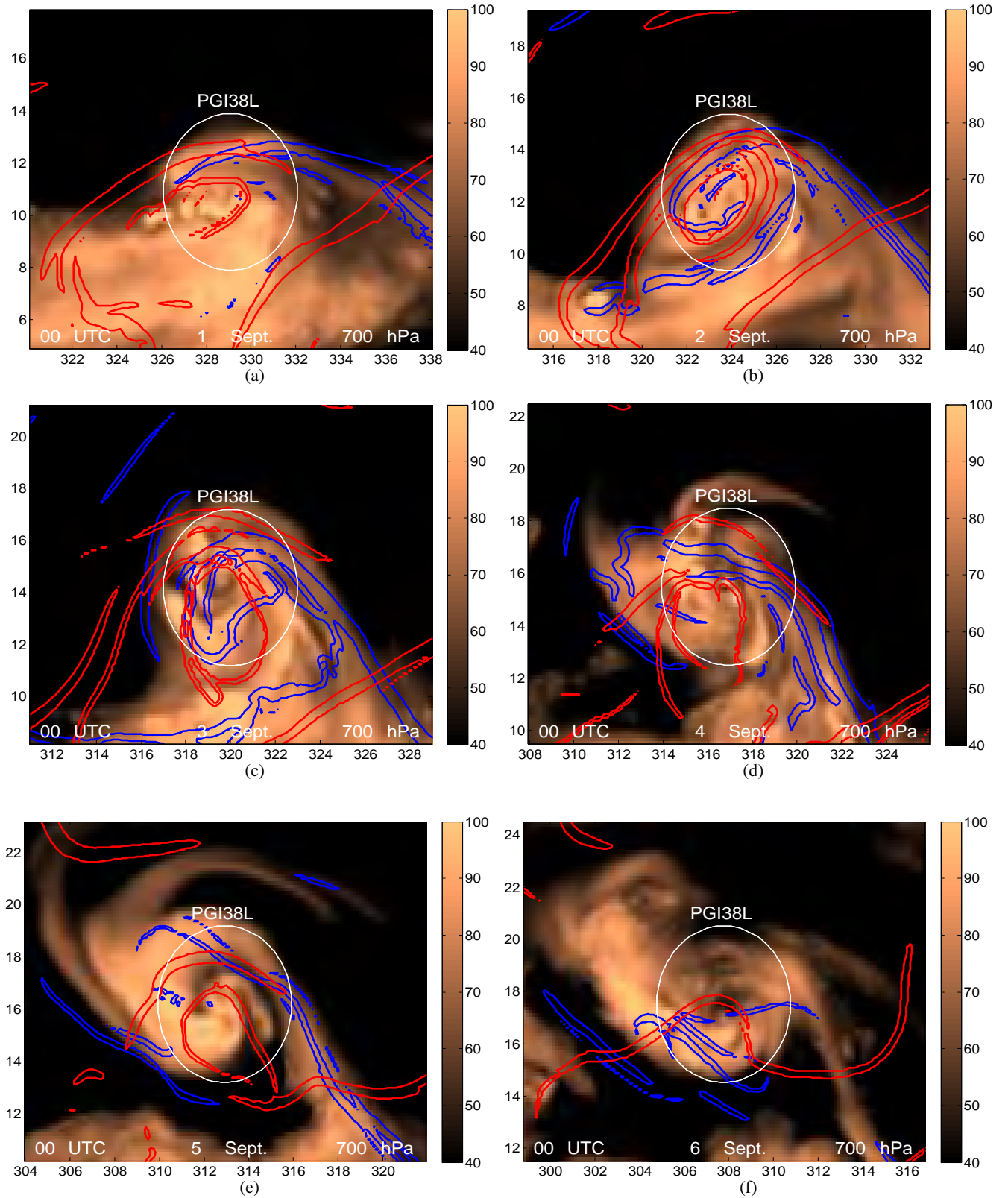
Fig. 10. Attracting LCSs (blue) and repelling LCSs (red) are overlaid on the relative humidity field at 700 hPa for ex-Gaston on Sept 1 (a), 2 (b), 3 (c), 4 (d), 5 (e) and 6 (f).
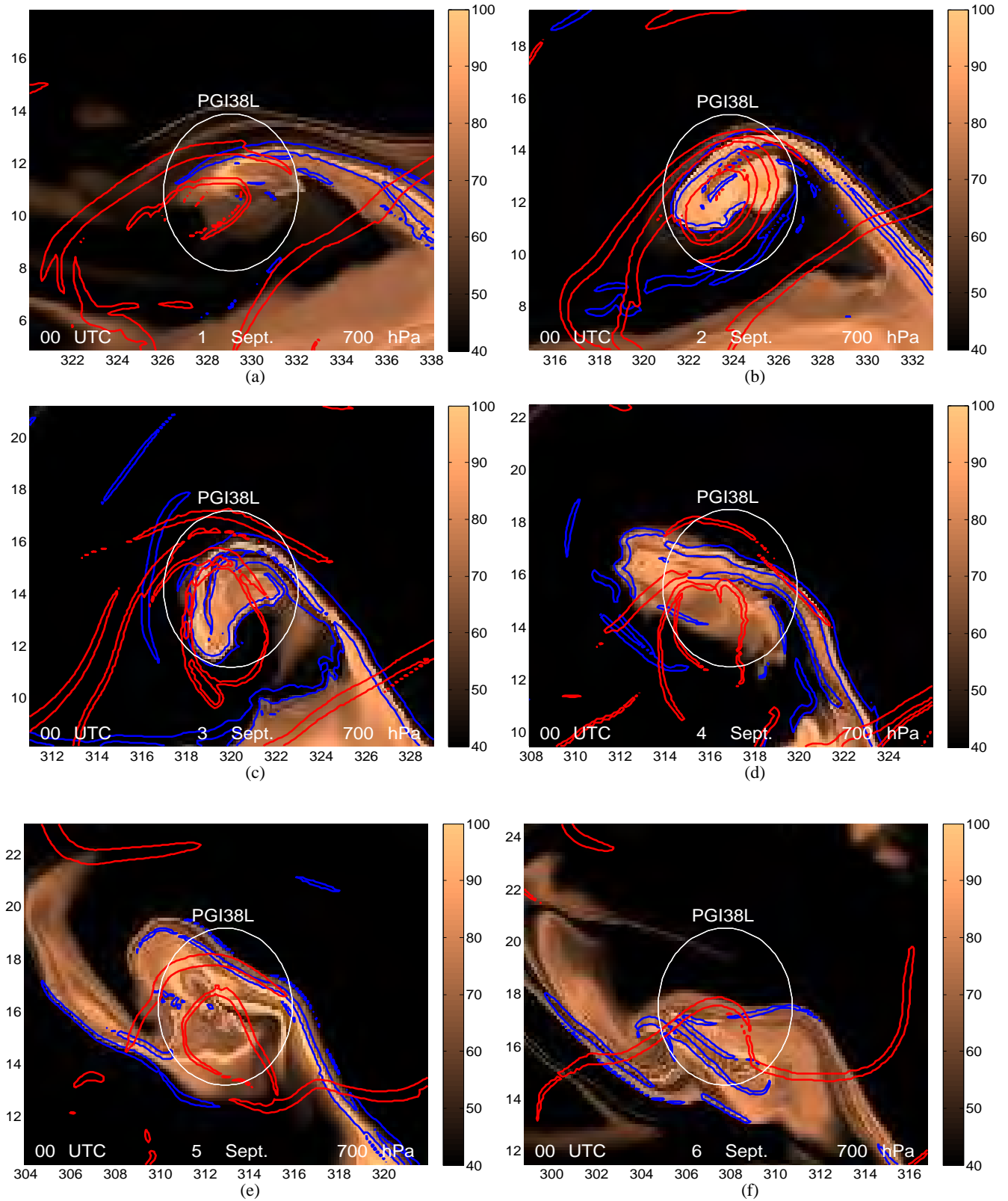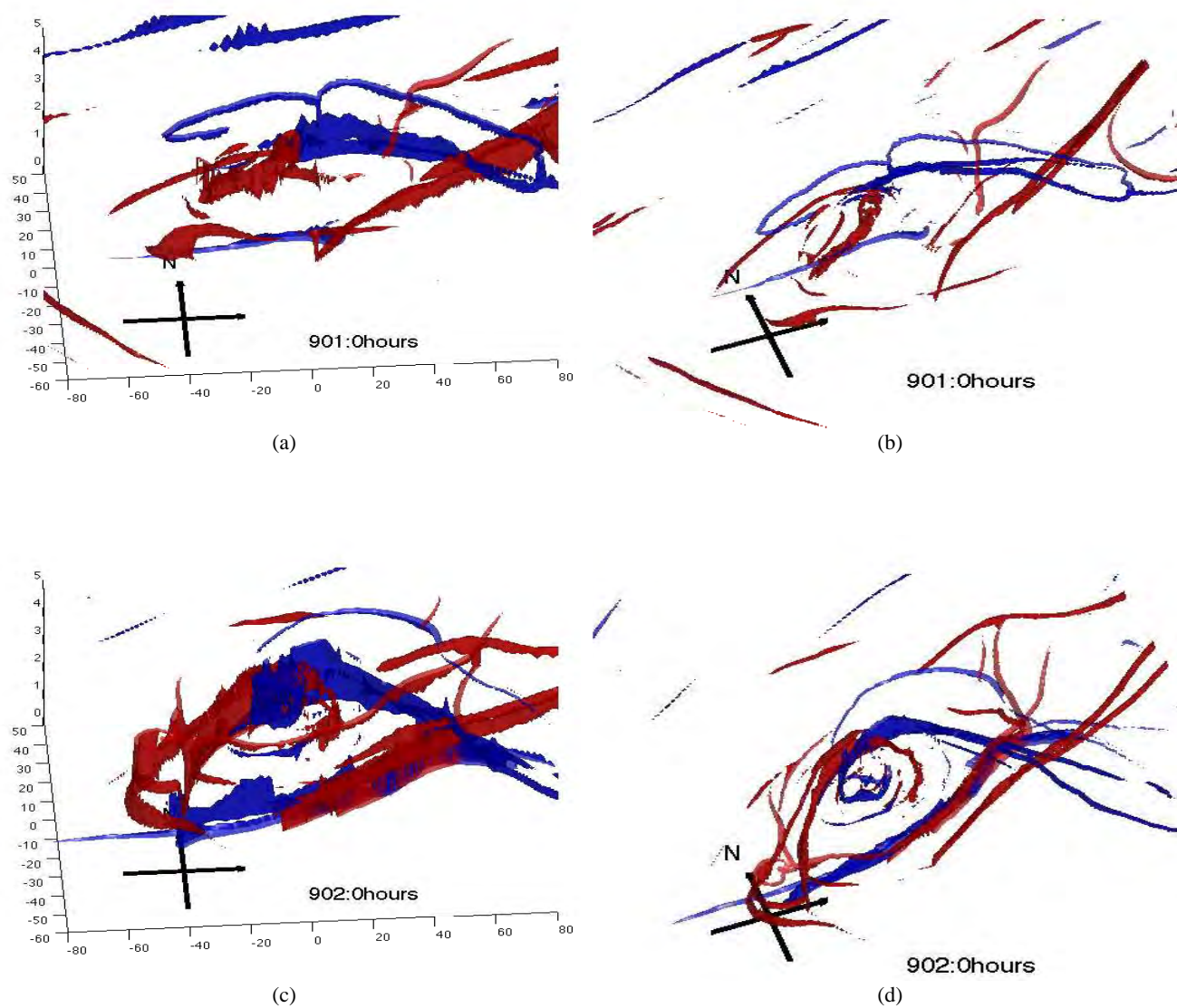
Fig. 11. Attracting LCSs (blue) and repelling LCSs (red) are overlaid on the relative humidity tracer field at 700 hPa for ex-Gaston on Sept 1 (a), 2 (b), 3 (c), 4 (d), 5 (e) and 6 (f).

Fig. 12. Attracting LCSs (blue) and repelling LCSs (red) are overlaid relative humidity tracer field at 500 hPa for ex-Gaston based on humidity values taken at particle locations on Sept 1 (a), 2 (b), 3 (c), 4 (d), 5 (e) and 6 (f).

Fig. 13. The vertical structure of ex-Gaston can be seen by 3D volume rendering of LCSs from 925 hPa to 500 hPa on Sept 1 (top) and Sept. 2 (bottom) looking due North (a, c) and from above (b, d).
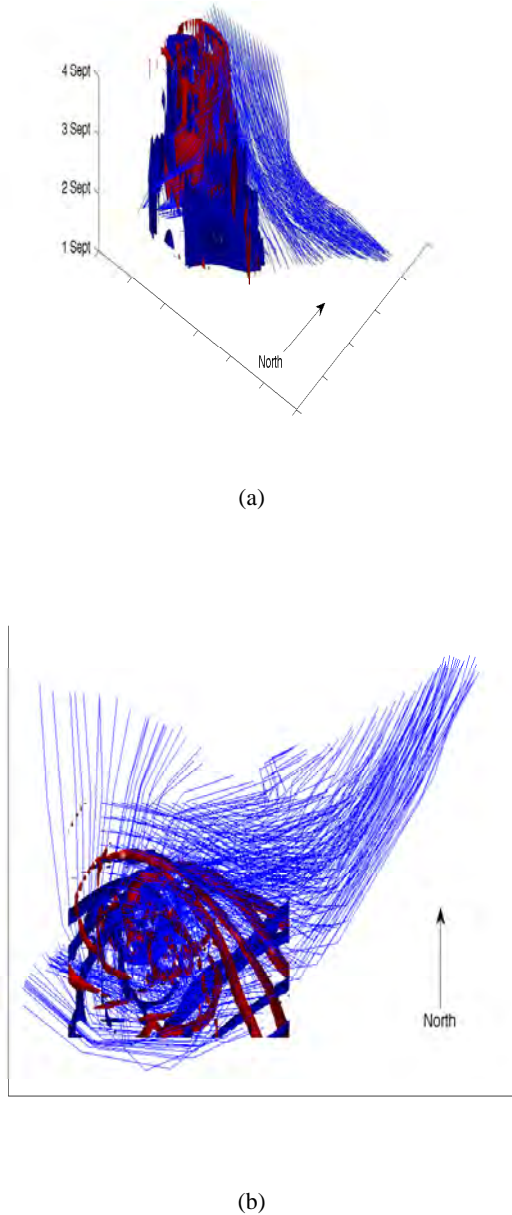
cal levels, Figures 8 and 9, in contrast to a disruption at 700 hPa and above for ex-Gaston. The average Lagrangian values increase as pre-Karl begins to develop on Sept. 15, as the LCSs form the boundaries of closed circulation.

6 Conclusions

In this study, we have introduced a new class of Lagrangian methods for time-dependent velocity fields to the study of tropical cyclogenesis. These methods were applied to developing tropical disturbances located along the wave trough axis of Easterly waves. The cat's eye boundary of the circulation was shown to be a robust feature even in the time-dependent context of the real tropical atmosphere. However, the time-dependent boundaries of the cat's eye, which control transport in and out of the cat's eye, were seen only by Lagrangian methods, and were not apparent in the Eulerian frame.

In this setting, the Lagrangian reference frame has advantages over both the Eulerian reference frame and translated Lagrangian frame. While the translated reference frame following the tropical disturbance showed closed streamlines, the Eulerian reference frame did not. However, streamlines from the translated frame were still crossed by trajectories. In contrast, the Lagrangian boundaries are based on particle trajectories, persistent through the time-variation, and are impermeable to particle trajectories.
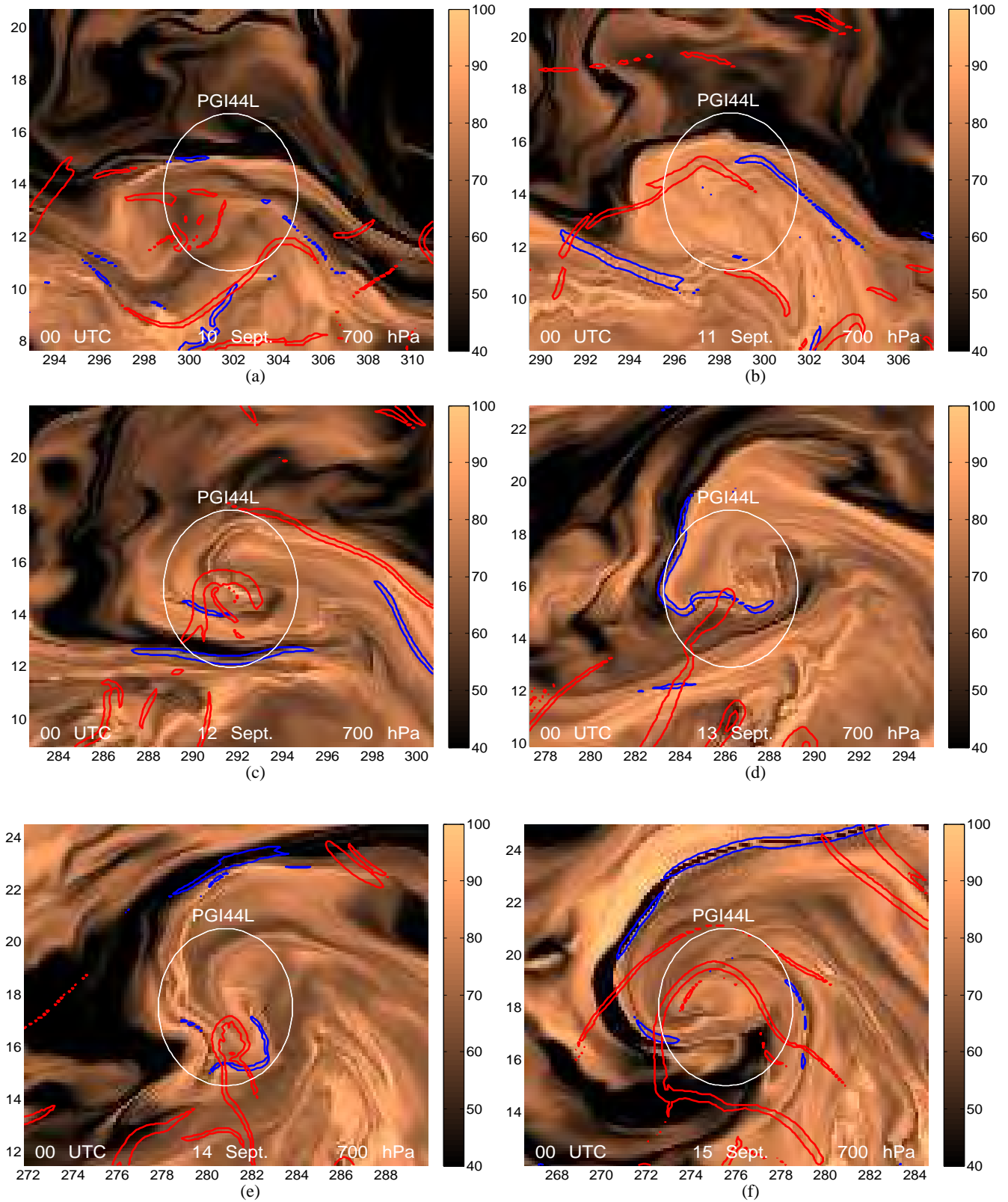
Attracting and repelling LCSs from FTLE fields were found in both a non-developing and developing disturbance to be the boundaries at the edge of the pouch associated with the cat's eye. The alignment and location of the LCSs defined pathways which determined the interaction of air masses with the tropical disturbance.

The Lagrangian fields were very different from Eulerian fields in the straining regions exterior to the vortex, and showed far more detail in which the actual pathways for moisture and vorticity transport could be seen. The important Lagrangian vortex boundaries occurred in regions of negative OW, outside of the Eulerian vortex boundary.

Lagrangian quantities were compared with common Eulerian quantities for diagnosing the strength of a candidate tropical disturbance. Averages of Lagrangian and Eulerian quantities similarly measure the strength of the disturbance, but the Lagrangian fields also show the structures responsible for changes in intensity.

Application to a developing and non-developing disturbance

The Lagrangian techniques were applied to a developing and non-developing disturbance observed during the PREDICT experiment. We have specifically examined the cases of ex-Gaston, which did not redevelop, and pre-Karl, which did develop into a hurricane. The LCSs showed boundaries which

(a)

(b)

Fig. 14. Backward trajectories are seeded on a 5 degree grid around the pouch center on Sept 4, and are integrated backward (thin blue curves) to Sept 1. Their planar locations are shown with attracting (red isosurface) and repelling (blue isosurface) LCSs with time increasing on the vertical axis from Sept 1 to Sept 4.

Fig. 15. Attracting LCSs (blue) and repelling LCSs (red) are overlaid on the RH tracer field at 700 hPa for pre-Karl at 700 hPa for Sept. 10 through Sept. 15.
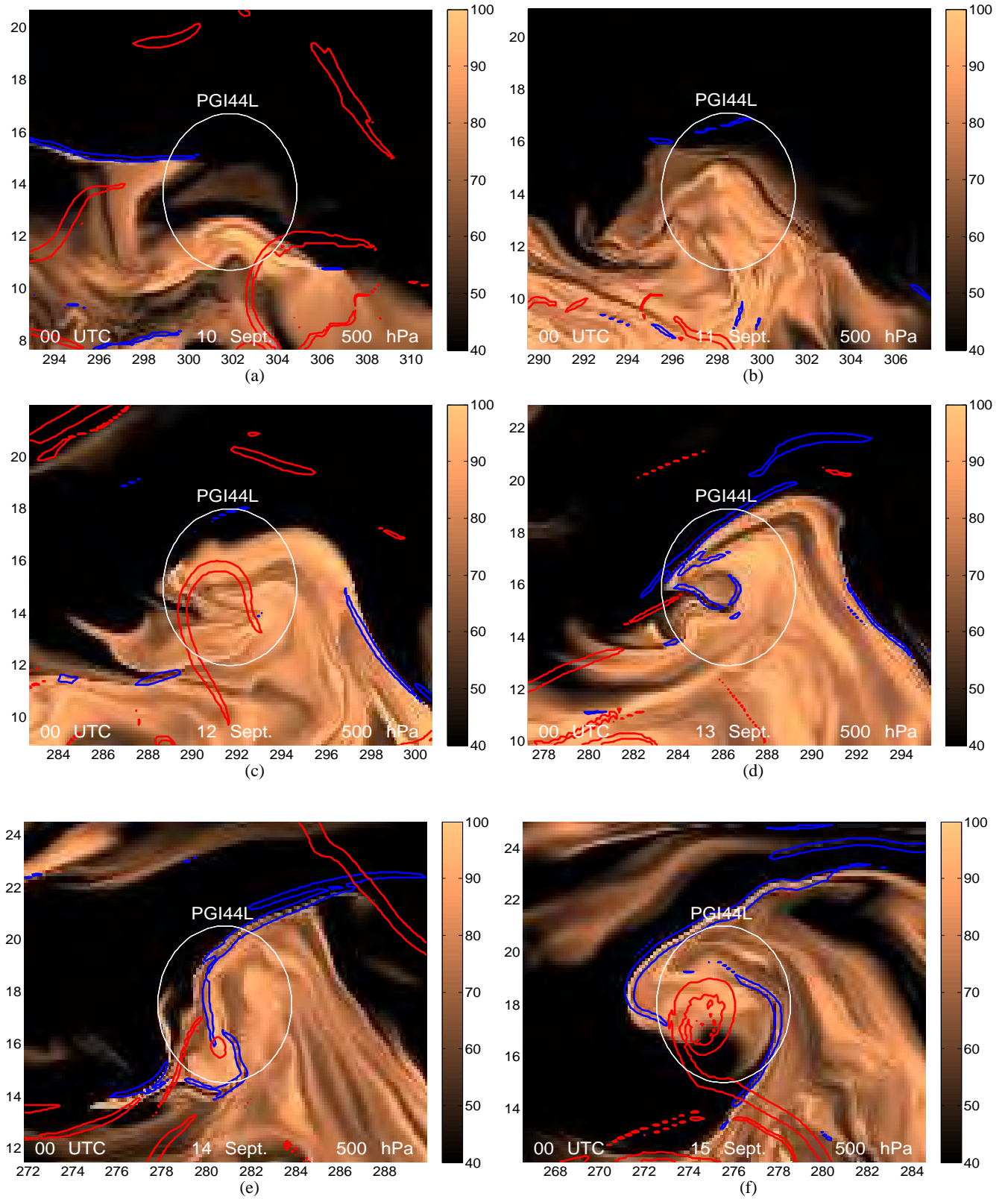
Fig. 16. Attracting LCSs (blue) and repelling LCSs (red) are overlaid on the RH tracer field at 500 hPa for pre-Karl from Sept. 10 to Sept. 15

constrained the transport of moisture and vorticity. Gaston and Karl had similar structure at lower levels of 850 hPa and below but were far different at 700 hPa and above. Gaston did not redevelop due to the intrusion of dry air, the expulsion of moist air with high vorticity, and a removal of a moisture source from the ITCZ. In addition, the presence of a repelling LCS in the inner core occurred as Gaston began to expel moist air. The LCSs showed the precise pathways and boundaries which were responsible for all of these processes. The LCSs for Karl were far more favourable for development. The LCSs blocked the intrusion of dry air, and retained a connection of moist air inflow from the ITCZ. A trajectory analysis showed the role of LCSs in organizing transport, and showed how Karl retained high moisture at all levels while Gaston did not.

Discussion and outlook

LCSs show both the planar pathways for stirring, and reveal a complete picture of the vertical structure of the wave-pouch region. While the planar mixing in these cases is supported by an analysis of thermodynamics (Smith and Montgomery , 2011), further study of the three-dimensional kinematics and flow boundaries will help to explain the roles of stirring and downdrafts for importing dry air and expelling moist air. The methods used in this study will be applied to additional pre-genesis cases from the 2010 PREDICT experiment to help identify the reasons for the development non-development of these pre-genesis cases. Real-time analysis using these methods will be explored also.

References

M. Branicki and S. Wiggins. Finite-time Lagrangian transport analysis: stable and unstable manifolds of hyperbolic trajectories and finite time Lyapunov exponents. Nonlinear Processes in Geophysics, 17:1–36, 2010.

C. Coulliette and S. Wiggins. Intergyre transport in a wind-driven, quasigeostrophic double gyre: An application of lobe dynamics. Nonlin. Proc. Geophys., 7:59–85, 2000.

C. A. Davis and D. A. Ahijevych. Mesoscale structural evolution of three tropical weather systems observed during PREDICT. J. Atmos. Sci., Submitted, 2011.

F. d'Ovidio, V. Fernandez, and E. Hernandez-Garcia. Mixing structures in the mediterranean sea from finite-size Lyapunov exponents. Geophy. Res. Lett., 31(17):L17203, 2004.

F. d'Ovidio, J. Isern-Fontanet, C. Lopez, E. Hernandez-Garcia, and E. Garcia-Ladona. Comparison between eulerian diagnostics and finite-size Lyapunov exponents computed from altimetry in the algerian basin. Deep-Sea Research I, 56:15–31, 2009.

J. Duan and S. Wiggins. Fluid exchange across a meandering jet with quasiperiodic variability. J. Phys. Oceanogr., 26:1176–1188, 1996.

T. J. Dunkerton, M. T. Montgomery, and Z. Wang. Tropical cyclogenesis in a tropical wave critical layer: Easterly waves. Atmos. Chem. Phys., 9:5587–5646, 2009.

C. Evans, H. Archambault, J. Cordeira, C Fritz, T. J. Galarneau Jr., S. Gjorgjievska, A. Griffin, K. andJohnson, W. Komaromi, S. Monette, P. Muradyan, B. Murphy, M. Riemer, J. Sears, D. Stern, B. Tang, and S. Thompson. The pre-depression investigation of cloud-sytems in the tropics (PREDICT) field campaign: Perspectives of early career scientists. Bull. Amer. Meteor. Soc., Accepted, 2011.

G. Haller. Finding finite-time invariant manifolds in two-dimensional velocity fields. Chaos, 10:99–108, 2000.

G. Haller. Distinguished material surfaces and coherent structures in three-dimensional fluid flows. Physica D, 149:248–277, 2001.

G. Haller. Lagrangian coherent structures from approximate velocity data. Physics of Fluids, 14:1851–1861, 2002.

G. Haller. An objective view of a vortex. J. Fluid Mechanics, 525:1–26, 2005.

G. Haller. A variational theory of hyperbolic Lagrangian Coherent Structures. Physica D, 240:574–598 (2011).

G. Haller and A. Poje. Finite time transport in aperiodic flows. Physica D, 119:352–380, 1997.

G. Haller and G. Yuan. Lagrangian coherent structures and mixing in two-dimensional turbulence. Physica D, 147:352–370, 2000.

Huber, M. and McWilliams, J. C. and Ghil, M. A climatology of turbulent dispersion in the troposphere Journal of the Atmospheric Sciences, 58:2377-2394, 2001.

K. Ide, D. Small, and S. Wiggins. Distinguished hyperbolic trajectories in time-dependent fluid flows: analytical and computational approach for velocity fields defined as data sets. Nonlinear Processes in Geophysics, 9(3/4):237–263, 2002.

G. Lapeyre, P. Klein, and L. Hua. Does the tracer gradient vector align with the strain eigenvectors in 2D turbulence? Physics of Fluids, 11 (12):3729–3737, 1999.

N. Malhotra and S. Wiggins. Geometric structures, lobe dynamics, and lagrangian transport in flows with aperiodic time-dependence, with applications to Rossby wave flow. J. Nonlinear Sci., 8:401–456, 1999.

A. M. Mancho, D. Small, S. Wiggins, and K. Ide. Computation of stable and unstable manifolds of hyperbolic trajectories in two-dimensional, aperiodically time-dependent vector fields. Physica D, 182:188–222, 2003.

M. T. Montgomery, C. Davis, T. J. Dunkerton, Z. Wang, C. Velden, R. Torn, S. J. Majumdar, F. Zhang, R. K. Smith, L. Bosart, J. S. Bell, M. M Haase, A. Heymsfield, J. Jensen, T Campos, and M. A. Boothe. The pre-depression investigation of cloud systems in the tropics (PREDICT) experiment: Scientific basis, new analysis tools and some first results. Bull. Amer. Meteor. Soc., Accepted, 2011.

C. O'Farrell and J. O. Dabiri. A Lagrangian approach to identifying vortex pinch-off. Chaos, 20:017513–1–9, 2010.

M. Riemer and M. T. Montgomery. Simple kinematic models for the environmental interaction of tropical cyclones in vertical wind shear. ACPD, 26:137–168, 2011.

B. Rutherford and G. Dangelmayr. A 3D Lagrangian hurricane eye-eyewall computation. Quart. J. Roy. Meteor. Soc.,

136:653:1931–1944, 2010.

B. Rutherford, G. Dangelmayr, and M. T. Montgomery. Lagrangian coherent structures in tropical cyclone intensification. preprint, 2011.

H. Salman, K. Ide, and C. K. R. T. Jones. Using flow geometry for drifter deployment in Lagrangian data assimilation. Tellus A., 60(2):321–335, 2008.

W. H. Schubert, M. T. Montgomery, R. K. Taft, T. A Guinn, S. R. Fulton, J. P. Kossin, and J. P. Edwards. Polygonal eyewalls, asymmetric eye contraction, and potential vorticity mixing in hurricanes. J. Atmos. Sci., 56:1197–1223, 1999.

S. Shadden. A dynamical systems approach to unsteady flows. PhD thesis, California Institute of Technology, 2006.

S. C. Shadden, F. Lekien, and J. E. Marsden. Definition and properties of Lagrangian coherent structures from finite-time Lyapunov exponents in two-dimensional aperiodic flows. Physica D, 212:271–304, 2005.

R. K. Smith and M. T. Montgomery. Observations of the convective environment in developing and non-developing tropical disturbances. Quart. J. Roy. Meteor. Soc., accepted, 2011.

W. Tang, M. Mathur, G. Haller, D. Hahn, and F. Ruggiero. Lagrangian coherent structures near a subtropical jet stream. J.Atmos.Sci., preprint, 2009.

J. B. Weiss and A. Provenzale. Transport and mixing in geophysical flows. Springer, 2008.